Mitomycin C and its analog trigger cytotoxicity in MCF-7 and K562 cancer cells through the regulation of RAS and MAPK/ERK pathways

Owen Zacarias, Cristina Clement, Shu-Yuan Cheng, Melissa Rosas, Christina Gonzalez, Marion Peter, Peter Coopman, Elise Champeil

Journal Pre-proof

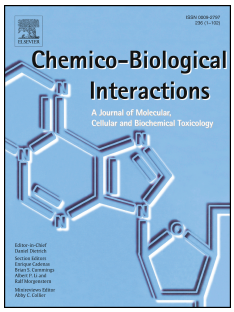

Mitomycin C and Its Analog Trigger Cytotoxicity in MCF-7 and K562 cancer cells through the regulation of RAS and MAPK/ERK pathways

Owen Zacarias, Cristina C. Clement, Shu-Yuan Cheng, Melissa Rosas, Christina Gonzalez, Marion Peter, Peter Coopman, Elise Champeil

PII: S0009-2797(24)00153-4

DOI: https://doi.org/10.1016/j.cbi.2024.111007

Reference: CBI 111007

To appear in: *Chemico-Biological Interactions*

Received Date: 23 January 2024

Revised Date: 27 March 2024

Accepted Date: 14 April 2024

Please cite this article as: O. Zacarias, C.C. Clement, S.-Y. Cheng, M. Rosas, C. Gonzalez, M. Peter, P. Coopman, E. Champeil, Mitomycin C and Its Analog Trigger Cytotoxicity in MCF-7 and K562 cancer cells through the regulation of RAS and MAPK/ERK pathways *Chemico-Biological Interactions*, https://doi.org/10.1016/j.cbi.2024.111007.

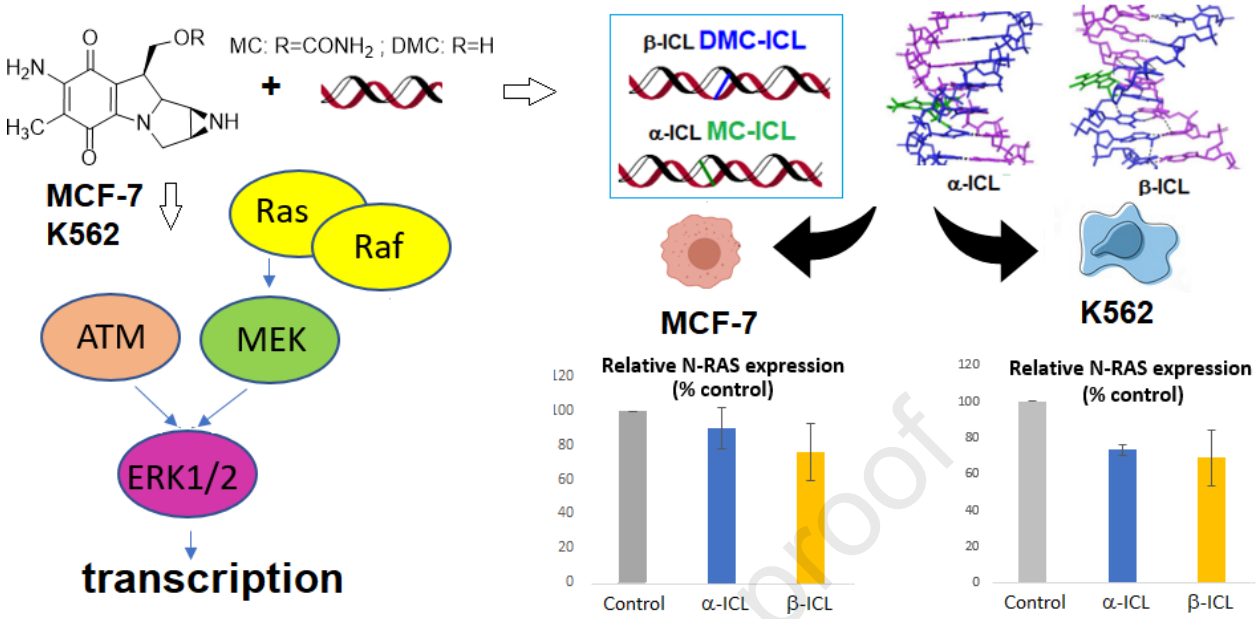

Mitomycin C and Its Analog Trigger Cytotoxicity in MCF-7 and K562 cancer cells through the regulation of RAS and MAPK/ERK pathways

Owen Zacarias[a,±], Cristina C. Clement[b*±], Shu-Yuan Cheng[a,c*], Melissa Rosas[a], Christina Gonzalez[a], Marion Peter[d], Peter Coopman[d], Elise Champeil[a,e*]

[a] *Department of Sciences, John Jay College of Criminal Justice, the City University of New York, New York, New York 10019 USA;* [b]*Radiation Oncology Department, Weill Cornell Medicine. New York, New York 10065, USA;* [c]*Ph.D. Program in Biochemistry, The Graduate Center of the City University of New York, New York, NY 10016 USA;* [d]*IRCM, University Montpellier, ICM, INSERM, CNRS, Campus Val d'Aurelle, 208 avenue des apothicaires, 34298, Montpellier, Cédex 5, France;* [e]*Ph.D. Program in Chemistry, The Graduate Center of the City University of New York, New York, NY 10016 USA*

CCC: 1300 York Avenue, E209/210, NY, 10065; 347-243-9023

ccc4002@med.cornell.edu

SYC: 524 West 59th Street, Room 05.61.09NB, New York, NY 10019; 646-557-4637; shcheng@jjay.cuny.edu

EC: 524 West 59th Street, Room 05.66.15NB, New York, NY 10019; 646-557-4502; echampeil@jjay.cuny.edu

± Both O. Zacarias and C.C. Clement share first authorship of this manuscript

Graphical Table of Content

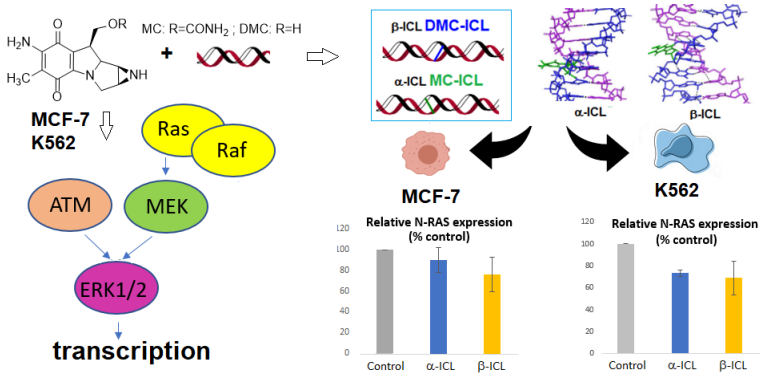

Title page

Title: **Mitomycin C and Its Analog Trigger Cytotoxicity in MCF-7 and K562 cancer cells through the regulation of RAS and MAPK/ERK pathways**

Short running title: Effect of Mitomycin C and 10-Decarbamoylmitomycin C on RAS

Authors: Owen Zacarias[a,±], Cristina C. Clement[b*±], Shu-Yuan Cheng[a,c*], Melissa Rosas[a], Christina Gonzalez[a], Marion Peter[d], Peter Coopman[d], Elise Champeil[a,e*]

Affiliation:

SYC, OZ, MR, CG and EC: Department of Sciences, John Jay College of Criminal Justice, the City University of New York, New York, New York 10019

SYC: Ph.D. Program in Biochemistry, The Graduate Center of the City University of New York, New York, New York 10016

MP, PC: IRCM, University Montpellier, ICM, INSERM, CNRS, Campus Val d'Aurelle, 208 avenue des apothicaires, 34298, Montpellier, Cédex 5, France

EC: Ph.D. Program in Chemistry, The Graduate Center of the City University of New York, New York, New York 10016

CCC: Weill Cornell medicine, New York, New York 10065

Corresponding authors:

Shu-Yuan Cheng, Cristina C. Clement and Elise Champeil

SYC: 524 West 59th Street, Room 05.61.09NB, New York, NY 10019; 646-557-4637; shcheng@jjay.cuny.edu

CCC: 1300 York Avenue, E209/210, NY, 10065; 347-243-9023; ccc4002@med.cornell.edu

EC: 524 West 59th Street, Room 05.66.15NB, New York, NY 10019; 646-557-4502; echampeil@jjay.cuny.edu

ABSTRACT

Mitomycin C (MC) is an anti-cancer drug which functions by forming interstrand crosslinks (ICLs) between opposing DNA strands. MC analog, 10-decarbamoyl mitomycin C (DMC), unlike MC, has stronger cytotoxic effects on cancer cells with TP53 mutation. We previously demonstrated that MC/DMC could activate $p21^{WAF1/CIP1}$ in MCF-7 (TP53-proficient) and K562 (TP53 deficient) cells in a TP53-independent mode. We also found that MC/DMC regulate AKT activation in a TP53-dependent manner and that AKT deactivation is not associated with the activation of $p21^{WAF1/CIP1}$ in response to MC/DMC treatment. RAS proteins are known players in the upstream mediated signaling of $p21^{WAF1/CIP1}$ activation that leads to control of cell proliferation and cell death. Thus, this prompted us to investigate the effect of both drugs on the expression of RAS proteins and regulation of the MAPK/ERK signaling pathways in MCF-7 and K562 cancer cells. To accomplish this goal, we performed comparative label free proteomics profiling coupled to bioinformatics/complementary phosphoprotein arrays and western blot validations of key signaling molecules. The MAPK/ERK pathway exhibited an overall downregulation upon MC/DMC treatment in MCF-7 cells but only DMC exhibited a mild downregulation of that same pathway in TP53 mutant K562 cells. Furthermore, treatment of MCF-7 and K562 cell lines with oligonucleotides containing the interstrand crosslinks (ICLs) formed by MC or DMC shows that both ICLs had a stronger effect on the downregulation of RAS protein expression in mutant TP53 K562 cells. We discuss the implication of this regulation of the MAPK/ERK pathway in relation to cellular TP53 status.

Keywords: Mitomycin C, 10-decarbamoyl mitomycin C, RAS pathway, Interstrand crosslinks, proteomic profiling

1. INTRODUCTION

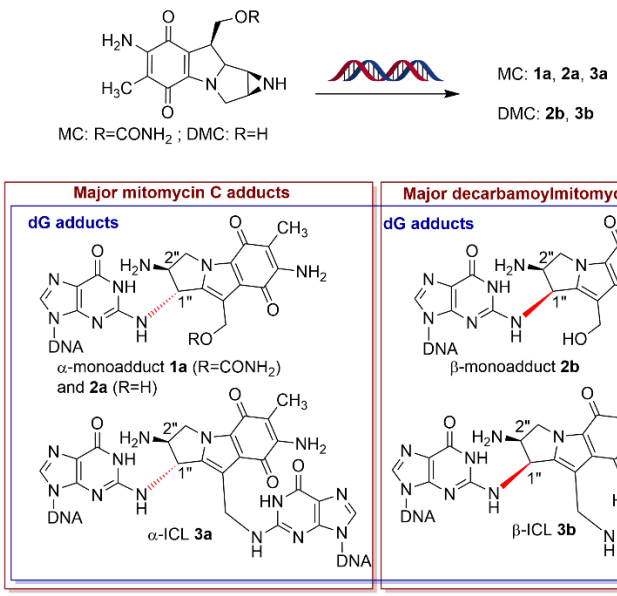

Figure 1: Major DNA adducts formed by MC and DMC in cancer cells. MC forms primarily *trans* (α) adducts at C1" and C2" (**1a**, **2a**, **3a**) and DMC *cis* (β) adducts (**2b**, **3b**).

Mitomycin C (MC)[1] is an anticancer agent used in cancer chemotherapy.[2-4] It is widely prescribed for the treatment of colorectal peritoneal metastasis (CPM).[5] MC, inert in its native form, alkylates cellular DNA monofunctionally and bifunctionally after reductive activation, resulting in the formation of deoxyguanosine monoadducts and interstrand crosslinks (ICLs) between two guanine bases on opposing DNA strands (Figure 1).[6-8] Interstrand crosslinks prevent DNA replication and, therefore, are highly cytotoxic to quickly proliferating cells. The presence of only 40 unrepaired ICLs is lethal to mammalian cells.[9] 10-Decarbamoyl mitomycin C (DMC) -a synthetic derivative of MC lacking the carbamoyl group- also forms ICLs in tumor cells.[10] The stereochemical configuration at C1'' of MC major monoadducts and ICL is *R* (**α or *trans***, Figure 1). In contrast, DMC generates preferentially the *S* stereoisomeric monoadducts and ICL (**β or *cis***, Figure 1). The crosslinking reaction is also diastereospecific with *trans*-crosslinks formed solely at CpG sequences, while *cis*-crosslinks are generated only at GpC

sequences.[11] Importantly, the *S* stereochemical configuration *(cis*) at C1" of the ICL produced by DMC correlates with the higher toxicity of DMC in human cancer cells compared to MC.[12-18]

Recent studies[13-18] have focused on the distinct cellular responses triggered by the two drugs. Treatment of MCF-7 cells with MC resulted in stabilization of TP53 protein as well as stabilization and increased mRNA transcription of p21, mdm2 and PUMA[15]; although $p21^{WAF1/CIP1}$ activation was later found to be TP53 and AKT independent whereas AKT deactivation was TP53 dependent.[17,18] DMC treatment of MCF-7 cells also led to TP53 protein stabilization as well as PUMA and $p21^{WAF1/CIP1}$ transcription but, contrary to MC, not to mdm2 activation, implying, perhaps, that the increased frequency or opposite stereochemical configuration of DMC-DNA adducts interferes with the ability of the basal transcription machinery to produce transcripts from the *mdm2* gene.[15] As with MC treatment, $p21^{WAF1/CIP1}$ activation was TP53 and AKT independent whereas AKT deactivation was TP53 dependent.[17-18]

There have also been reports, albeit less extensive, on the effects of both mitomycins on TP53-mutant K562 cells. These studies have shown that unlike MC, DMC triggered PARP cleavage and caspase activation which are markers of apoptosis [13-16]. With both drug treatments, $p21^{WAF1/CIP1}$ was activated and there was no AKT deactivation.

Earlier results showed that DMC is more toxic against cells lacking a functional TP53 than MC. At least nine different cell lines have been used to investigate the cytotoxicity of MC/DMC in relation to TP53 status including ML-1[14], K562[14], MCF-7[14], p53 shRNA MCF-7[13], DLD-1[15], DA-2[15], EMT-6[12], MDA-MB-468[19] and MCF-10A[19]. Overall, results suggest that contrary to MC, which forms primarily the α-ICL, DMC, which produces mainly the β-ICL, can trigger a TP53-independent form of cell death.[16] This has clinical relevance because more than 50% of cancers have a mutated TP53 gene. Accordingly, understanding which ICL structural

features are responsible for the TP53-independent cell death triggered by mitomycins will lead to the design of more efficient chemotherapeutics targeted to cancer cells with a mutant TP53. Our overarching goal is to decipher the molecular mechanisms responsible for the control of proliferation and cell death triggered by MC and DMC in cancer cells with or without a functional TP53 gene. We previously showed that both MC/DMC and the α-ICL produced by MC activate $p21^{WAF1/CIP1}$ by triggering dephosphorylation of $p21^{WAF1/CIP1}$ at p-Thr145 in MCF-7 cells (WT TP53). MC and DMC are also able to activate $p21^{WAF1/CIP1}$ in K562 cells (mutant TP53)[17]. However, the upstream signaling of $p21^{WAF1/CIP1}$ remains unidentified.

Literature points to RAS as a likely actor in the upstream signaling of $p21^{WAF1/CIP1}$ activation in the control of cell proliferation and cell death.[20] RAS proteins are GTPase enzymes which exist as four isoforms: KRAS4A and 4B (Kirsten RAS), HRAS (Harvey RAS) and NRAS (Neuroblastoma RAS). One of their main roles is to transduce extracellular signals from membrane receptors (such as EGF-R: Epidermal Growth Factor Receptor) to the nucleus.[20] RAS proteins have been the focus of intensive research in the past 40 years.[20,21] These studies have demonstrated that they are involved in the control of cell proliferation, but the molecular mechanisms by which they send mitogenic cues to promote cell growth or proliferation have not been totally elucidated yet. The most studied immediate effectors of RAS activation are the members of the MAPK signaling cascade.[22-24] Further studies have identified the TP53/$p21^{WAF1/CIP1}$ axis as a crucial intermediary in the RAS mitogenic pathway. Importantly, these studies have established that RAS signaling does not affect the levels of TP53 expression, but that it totally impedes $p21^{WAF1/CIP1}$ expression[25] and that ERK2 activation transduces mitogenic signals, at least in part, by downregulating the cell cycle inhibitory protein $p21^{WAF1/CIP1}$.[26] Additional genetic research has determined that the TP53/$p21^{WAF1/CIP1}$ axis is

central to the mitogenic pathway which links RAS signaling to the cell cycle machinery. However, it has also been shown that cells with typical RAS proteins but missing a functional TP53/p21$^{WAF1/CIP1}$ axis do not multiply without signaling through RAS.[25]

The research presented here is the first to shed new light on the modulation of RAS/ERK activity mediated by MC/DMC treatment as well as by the interstrand crosslinks formed by each drug in MCF-7 and K562 cancer cells. This study is a necessary step to uncover the link between ERK/MAPK signaling and potential downstream effect on TP53 independent p21$^{WAF1/CIP1}$ activation leading to the inhibition of cancer cell proliferation. To reveal the molecular mechanisms involved in the regulation of ERK/MAPK signaling by the two mitomycin drugs and by the ICLs they form, we employed comparative global and quantitative label-free proteomics analysis of relative changes in the protein abundance and expression profiles in MCF-7 and K562 cancer cells treated with 50 μM of MC/DMC or 10 nM of the α/β-ICL. We validated the changes in the expression of RAS, ERK and pERK protein using western blot analysis and investigated the level of phosphorylated proteins in the RAS/MAPK/ERK pathway and the well-described crosstalk JAK/STAT[27,28] mediated signaling axis by means of phosphoproteomics arrays.

Our results revealed molecular signatures that modulate the downregulation of MAPK/ERK pathway upon MC/DMC treatment in MCF-7 cells. However, in the case of TP53 mutant K562 cells, only DMC mediated the downregulation of the MAPK/ERK pathway. In addition, treatment of MCF-7 and K562 cell lines with oligonucleotides containing the interstrand crosslinks (ICLs) formed by MC or DMC showed that both ICLs had a stronger effect on the downregulation of RAS protein expression in mutant TP53 K562 compared to WT TP53 MCF-7 cells. Notably, only the β-ICL formed by DMC induced the downregulation of the

MAPK/ERK pathway in TP53 mutant K562 cells. This study paves the way for the investigation of molecular mechanisms linking RAS signaling and TP53 independent activation of $p21^{WAF1/CIP1}$ (leading to the inhibition of cancer cell proliferation) upon cancer cells treatment with drugs generating structurally different ICLs.

2. MATERIALS AND METHODS

2.1 Cell culture and reagents

Human breast cancer MCF-7 (p53-proficient) and human chronic myelogenous leukemia K562 (p53-deficient) cell lines obtained from American Type Culture Collection (Manassas, VA, USA) were used in this study. MCF-7 cells were cultured within Dulbecco's modified eagle's medium (DMEM) with 10% fetal bovine serum (FBS), and 50 µg/ml gentamycin. K562 cells were cultured within RPMI1640, 10% FBS, 2 mM glutamine and 50 µg/ml gentamicin. Cell culture reagents such as DMEM, RPMI 1640, FBS and gentamicin were obtained from Thermo Fisher Scientific (Waltham, MA, USA). Both cell lines were maintained in an incubator at 37°C with 5% CO_2. On the day before chemical exposure, cells were cultured into 60 mm Petri dishes or flasks. Cells with about 80% confluence were then ready for chemical exposure.

Mitomycin C (MC) was a generous gift from Prof. M. Tomasz. 10-Decarbamoyl mitomycin C (DMC) was synthesized following Kinoshita's protocol.[29]

Mammalian Protein Extraction reagent (M-PER) and Halt protease/phosphatase inhibitor cocktail were obtained from Pierce (Rockford, IL, USA). Protein concentration was determined by detergent compatible Bio-Rad DC (Hercules, CA, USA). β-actin antibody was obtained from Sigma-Aldrich (St. Louis, MO, USA). All other antibodies were from Santa Cruz Biotechnology (Dallas, TX, USA). Western blot analysis reagents, such as Super Signal West Pico

chemiluminescent kit, anti-rabbit IgG or anti-mouse IgG secondary antibodies conjugated to horseradish peroxidase as well as stripping buffer were obtained from Pierce (Rockford, IL, USA). Trifluoroacetic acid, iodacetamide, RIPA buffer, Triton X-100, TCEP-HCL (Tris (2-carboxyethyl) phosphine hydrochloride), phosphatase inhibitor cocktail 2, phosphatase inhibitor cocktail 3, sodium citrate, fetal bovine serum (FBS), glycerol and beta-glycerophosphate, disodium salt, pentahydrate were all purchased from Millipore-SIGMA-Aldrich (St. Louis, MO, USA). Acetonitrile Optima™ LC/MS, acetic acid, formic acid Optima™ LC/MS, HEPES Buffer, methanol Optima™ LC/MS and Tris-HCl were all purchased from Fisher Scientific (Pittsburgh, PA, USA). Urea, dithiothreitol (DTT), ultrapure EDTA (0.5 M solution, pH 8.0), ammonium bicarbonate, potassium chloride, monobasic potassium phosphate, phosphoric acid, HPLC-grade water and micro-BCA protein assay kit were all purchased from ThermoFisher Scientific (Waltham, MA USA). Trypsin, Lys-C and GluC, all sequencing grade purity were purchased from Promega (Madison, WI, USA).

2.2 Chemical treatment

MC and DMC solutions at various concentrations were prepared 15 minutes before experiments in cell culture media. Concentrations were based on previous studies.[17,18] Cells treated with chemicals were incubated at 37ºC for 24 hours. Cells transfected with the ICLs were incubated in a10 nM final α/β-ICL concentration per Petri dish for 24 hours at 37ºC. The transfection protocol is detailed in section 2.8.

2.3 Western blot analysis

After chemical treatments, cells were lysed with M-PER lysis buffer supplemented with Halt protease/phosphatase inhibitor cocktail following the manufacturer's protocol. Protein concentration was determined by Bio-Rad DC reagents using bovine serum albumin (BSA) to set

up a calibration curve. Western blot analysis was performed as previously described.[18] Briefly, 40 µg of total proteins from cell lysates were subjected to 4-20% Mini-Protean TGX gels (Bio-Rad) for protein separations via SDS-PAGE electrophoresis. After separation, proteins were then transferred onto polyvinylidene fluoride (PVDF) membranes for immunoblotting. Membranes were blocked with 5% BSA in phosphate buffered saline (PBS) and 0.05% Tween20 (5% BSA in PBS/0.05%Tween 20) for 1 hour at room temperature with shaking. Membranes were then incubated with primary antibody at 1 µg/µl overnight at 4ºC with shaking. After incubating with primary antibody, corresponding horseradish peroxidase-linked secondary antibody was applied for 1 hour at room temperature with shaking. Membranes were developed using Super Signal West Pico Chemiluminescent Substrate detection reagents. Chemiluminescent signals were captured using ChemiDoc Imaging System and analyzed by Image Lab Software (Bio-Rad). After obtaining the data for the first target protein, membranes were then stripped with Stripping buffer for 15 minutes at room temperature and re-probed with β-actin (1 µg/µl) and ERK antibodies (1 µg/µl) as the loading control.

2.4 Protein expression profiles of MCF-7 and K562 cells treated with MC and DMC

Proteomics profiling analysis was performed by means of a label-free quantitation (LFQ) method using modified protocols originally described in detail in other proteomics research papers.[30,31] The comprehensive comparative proteomics profiling of MCF-7/K562 treated with MC, DMC and the ICLs will be the subject of a future manuscript. We report herein the key findings regarding the modulation of MAPK/ERK signaling pathway in MCF-7/K562 cells treated with MC and DMC and the α/β-ICLs.

2.4.1 Sample preparation and nanoLC-MS/MS

Total protein concentration from each total cell lysate obtained from the control or drug treated MCF-7 and K562 cells samples was determined using Bradford micro assay. Equal protein amounts (50 µg), prepared in technical triplicates, were reduced in 25 mM DTT (Thermo Scientific) in 50 mM ammonium bicarbonate buffer, at pH 8.5, for 55 minutes at 55ºC. The reduced proteins were further alkylated with 150 mM iodoacetamide solution, in the dark, for 50 minutes at room temperature. Three different enzymes were used for "in solution" digestion in 50 mM ammonium bicarbonate buffer, pH 8.5, for 18 hours, at 37 °C: endoproteinase Lys-C (1:50 enzyme: protein ratio); trypsin (1:20 enzyme: protein ratio) and Glu-C (1:10 enzyme: protein ratio) (sequencing grade Promega, Madison, WI, USA). The peptides mixture, extracted from all enzymatic digestions, were desalted on C18 Prep clean columns before high resolution liquid chromatography tandem mass spectrometry (LC-MS/MS). The reversed-purified peptide mixtures from n=3 or n=4 independent treatment experiments were subjected to nanoLC-MS/MS sequencing on a Q Exactive HF quadrupole orbitrap mass spectrometer with an ESI nanospray source (Thermo Fisher Scientific, Waltham, MA, USA) using the protocols and services provided by Creative Proteomics, NY, USA (www.creative-proteomics.com). The mass spectrometer was operated in a positive ion mode and in data-dependent acquisition (DDA) mode with the following settings: full MS scans were obtained within a 300 to 1650 m/z range with a mass resolution of 60,000 at m/z 200, and a target value of 1.00E+06 with a maximum injection time of 19 ms. HCD collision was performed on the top 20 most significant peaks, and tandem mass spectra were acquired at a mass resolution of 15,000 at m/z 200 and a target value of 1.00E+05. Isolation of precursors was performed with a window of 1.4 Th. The dynamic exclusion time was 30s. The normalized collision energy was 28%. We excluded precursor ions with single, unassigned, or six and higher charge states from fragmentation selection.

2.4.2 Protein identification

Raw files from each technical and biological replicate were filtered, de novo sequenced and assigned with protein ID using Peaks X/X+ and XPro software (Bioinformatics Solutions, Waterloo, Canada, ON), by searching against the human *(Homo sapiens)* Swiss-Prot reviewed database (March 2021; 20385 entries). The following search parameters were applied for LFQ analysis: for each LysC, trypsin and GluC we allowed one missed cleavage at one peptide end. The parent mass tolerance was set to 18 ppm using monoisotopic mass, and fragment ion mass tolerance was set to 0.05 Da. Carbamidomethyl cysteine (+57.0215 on C) was specified in PEAKS 8.0 as a fixed modification. Methionine, lysine, proline, arginine, cysteine and asparagine oxidations (+15.99 on CKMNPR), deamidation of asparagine and glutamine (NQ-0.98) and pyro-Glu from glutamine (Q-18.01 N-term) were set as variable modifications. Data were validated using the FDR method built in PEAKS X/X+ and XPro and protein identifications were accepted with a confidence score (-10lgP)>15 for peptides and (-10lgP)>15 for proteins; a minimum of 1 peptide per protein after data were filtered for less than 3.0 % FDR for peptides and less than 4% FDR for protein identification ($p<0.05$). An independent validation of the MS/MS-based peptides and protein identification was performed with Scaffold (version Scaffold_4.5 and higher, Proteome Software Inc.) using the compatible ".mzid" files of all samples exported from PEAKS X/X+/Xpro. Peptide identifications were accepted if they could be established at greater than 95.0% probability by the Peptide Prophet algorithm with Scaffold delta-mass correction. Protein identifications were accepted if they could be established at greater than 95.0% probability and contained at least 1 identified peptide.

2.4.3 Label-free relative peptide quantification (LFQ)

The PEAKS Q module implemented in the PEAKS X/X+/XPro proteomics software (Bioinformatics Solutions, Waterloo, Canada, ON) was applied to assess the differential protein expression profiles in MCF-7 and K562 cells treated with 50 μM MC/DMC and 10 nM α/β-ICLs for 24 hours. Relative protein abundances profiles were extracted from MS1 areas in PEAKS X/X+/XPro proteomic software using the LFQ module. Normalization was performed using the corresponding averaged MS1 areas (i.e. abundances) with respect to the total ion current (TIC) and with respect to the total abundance of actin, which showed no changes during drug treatment. The protein fold changes were calculated by rescaling their values using a log2 transformation. The complete analysis of proteomics data is presented in the Supporting Information (Supplementary table S1).

2.4.4 Gene ontology (GO), molecular and cellular pathways enrichment analysis

Networks, functional analyses, biochemical and cellular pathways were generated using the Ingenuity Pathway Analysis (IPA; Ingenuity Systems, Redwood City, CA, USA) and the list of proteins extracted from PEAKS DB searches, together with their experimentally determined ratios corresponding to the protein MS1 areas (abundances) extracted from the LFQ analysis in the PEAKS software. Specifically, the abundance ratios corresponding to each quantifiable protein from drugs and ICLs treated MCF-7 and K562 cells vs control, untreated samples, were used to calculate the experimental fold changes by rescaling their values using a log2 transformation, such that positive values reflected fold increases while the negative values reflected fold decreases. For network generation, datasets containing gene identifiers (gene symbols) were uploaded into the IPA application together with their rescaled log2 transformation of protein's area ratios. These molecules were overlaid onto a global molecular network contained in the Ingenuity Knowledge Base. The networks were then algorithmically generated

based on their connectivity index using the built-in IPA algorithm. The probability of having a relationship between each IPA indexed biological function and the experimentally determined genes were calculated by a right-tailed Fisher's exact test. The level of significance was set to a P-value of <0.05. Accordingly, the IPA analysis identified the molecular and cellular pathways from the IPA library of canonical pathways that were most significant to the dataset (-log (p value)>2.0). For the quantitative analysis of the expression profiles, IPA assigned a "z-score" function to all eligible canonical and cellular pathways (where a "$z \leq -1.5$" represents significant down-regulation while a $z \geq 1.5$ represents a significant up-regulation of the selected pathway). The proteins associated with the canonical MAPK/ERK signaling pathway were assigned to each proteome data set using the IPA related database and are presented in the Supporting Information (Supporting documents S.2.1 to S.2.8).

2.5 Targeted analysis of key signaling phosphoproteins regulating the cancer pathways in MCF-7 and K562 cancer cell lines treated with MC and DMC

The semi-quantitative detection of phosphorylated human proteins in the MAPK/ERK and JAK/STAT signaling pathways in the cell lysates from the untreated (control) and MC, DMC treated MCF-7 and K562 samples was performed using the RayBio® C-Series Human Phosphorylation Multi-Pathway Profiling Array C55 (Cat# AAH-PPP-1-8) and following the manufacturer instructions. About 100 μg of total protein lysates from each sample set was loaded on each provided array membrane, probed accordingly to technical instructions and developed using chemiluminescence then further quantified in ImageJ. Once the raw numerical densitometry data was extracted in ImageJ, the background was subtracted, and the data were normalized to the Positive Control signals for each array. *Positive Control Normalization*: the amount of detection antibody printed for each positive control spot is consistent from array to

array. As such, the intensity of these positive control signals is used to normalize signal responses for comparison of results across multiple arrays. The details of normalization and the final relative quantitative data calculations for each phosphoprotein displayed for each pathway are presented in the Supporting information (Supplementary table S3). An independent analysis was performed with the apoptosis antibody arrays purchased from Fullmoon biosystem (Sunnyvale, CA, USA). Results of the assays were analyzed by the company. For each spot on the array, median signal intensity (i.e., median value of average signal intensity for all antibodies on the array, excluding positive marker and negative control) is extracted from the array image. Average signal intensity of replicate spots is the mean value of median signal intensity of the replicate spots for each antibody. The CV refers to the coefficient of variation for each antibody's replicate spots. Data are normalized as follows: average signal intensity of replicate spots / median signal normalized. Fold change between control and treatment samples from normalized data is determined as follows: Treatment sample/control sample.

2.6 Statistics

The results are reported as means ± SEM of at least 3 independent experiments. Statistical significance was determined using one-way analysis of variance (ANOVA) followed by Dunnett's post-hoc test ($p<0.05$, with control at 100%) using the GraphPad PRISM®8 (or higher version) software for LFQ analysis of proteomics data. The Student's T-Test was applied for assessing the significance of western blots data. Data from the protein arrays were analyzed using the two-tailed unpaired one-way analysis of variance (ANOVA) with uncorrected Fishers' LSD test or two-way ANOVA followed by multiple comparison tests and Holm-Sidak method. Results were weighted for their statistical significance based on the calculated p-values as follows: $p \leq 0.05$ (*); $p<0.01$ (**); $p<0.001$ (***) and $p<0.00001$ (****).

2.7 Synthesis of duplex oligonucleotides bearing a single ICL at a specific site

Both syntheses are previously described by us.[32,33]

2.7.1 α-ICL and tagged α-ICL synthesis

Synthesis of the α-ICL: Briefly, the 25-mer 5'-TCCTCCTATTATTCGTATTCCTCCT-3' was annealed to the 12-mer 5'- AATAC$^{5\text{-Me}}$GAATAA-3' and then reacted with reduced MC (4 mmol/mL) using a sub-stoichiometric amount of sodium dithionite to generate the α-monoadduct. The monoalkylated 25-mer was isolated by HPLC. The α-ICL was generated by hybridizing the MC-mono-adduct-containing 25-mer with its complementary strand, and the duplexes underwent further cross-linking by addition of sodium dithionite. The 25-mer duplex containing the α-ICL was purified by PAGE. The tagged α-ICL was generated by hybridizing the monoadducted 25-mer with a complementary strand bearing the 5' modification (5'-amino C6-AF594 fluorophore, Midland Certified Reagent Company, Midland, Texas) tethered to the oligonucleotide via a 6 carbon atom alkyl chain. The duplex underwent further cross-linking by addition of $Na_2S_2O_4$ and the tagged α-ICL was purified by PAGE and characterized by UV-vis, enzymatic digestion and mass spectroscopy (Supporting information S4).

2.7.2 Synthesis of the β-ICL

Briefly, the 25-mer 5'-TCCTCCTATTATTGCTATTCCTCCT-3' was annealed to a 12-mer 5'- AATAGCAATAA-3' and the duplex was reacted with fully reduced DMC (generated using excess sodium dithionite) at 0° C to generate the β-monoadduct. This reaction sequence (from annealing to addition of fully reduced DMC) was repeated with the same starting materials three times. The β-monoadduct was isolated by HPLC and the β-ICL was generated by hybridizing the 25-mer 1"-β monoadduct with its complementary strand and reducing the

quinone moiety with Na_2SO_4 to trigger the second arm alkylation and convert the monoadduct into the β-ICL at 42°C. The final β-ICL was isolated by PAGE.

2.8 Cell transfection

α/β-ICLs and tagged α-ICL (0.5 µg, 0.03 nm i.e. 5.0 µL from a 6.1 µM solution in water) were diluted into Opti-MEM (480 µL, Gibco). Interferin (10 µL, Polyplus, Illkirch, France) was added. The mixture was vortexed (10 s) and incubated for 20 minutes to allow for complexation then transferred into a well of a 6-well plate. MCF-7 and K562 cells (500,000 per well) were seeded, and the volume was adjusted to 3 mL (complete medium) resulting in a 10 nM final α/β-ICL concentration per well.

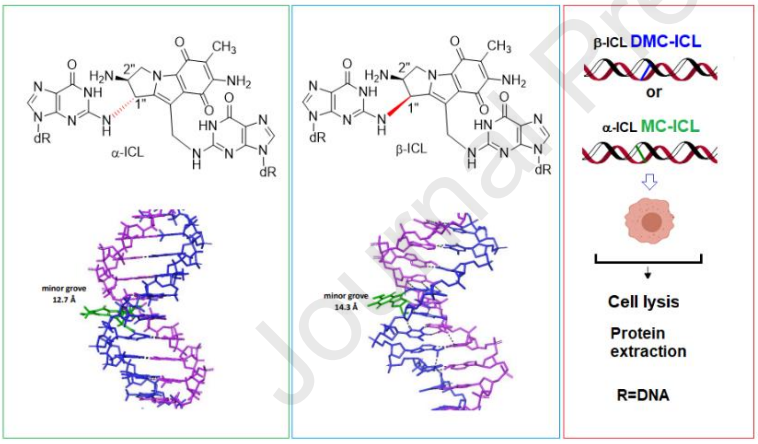

Figure 2: Transfection of DNA adducts formed by MC and DMC in MCF-7 cells.

2.9 Fluorescence microscopy

MCF-7 cells stably expressing H2B-GFP[34] were cultured in DMEM containing Glutamax and complemented with 10% FBS complete medium (Eurobio, Les Ulis, France) and G418 (0.8 mg/mL, InvivoGen) in a humidified atmosphere at 37°C and 5% CO_2. Two hours or 23 hours after transfection, a mitochondrial staining reagent (3 mL, blue Cytopainter, Abcam, Boston, MA)

prepared according to the manufacturer's protocol was added to the plated cells that were further incubated for an hour with a total incubation time of 3 or 24 hours. Fixation was accomplished by directly adding paraformaldehyde (Electron Microscopy Sciences) to each well for a 4% final concentration followed by a 15 minutes incubation at room temperature. Cells were then washed twice with PBS and the coverslips were mounted with ProLong Gold (Fisher Scientific, Waltham, MA). Samples were examined with a Zeiss Axio Imager M2 microscope equipped with the ApoTome.2 system and a Zeiss 40X/1.3 oil Plan-Apochromat objective. Images were acquired using a Hamamatsu Orca-Flash4.0 camera controlled with Zen 3.3 software. Three-dimensional image stacks throughout the cells (10 µm range, 1 µm interval) were captured with the ApoTome and processed using Fiji software.[35]

3. RESULTS

3.1 Localization of ICLs after cell transfection

Figure 3 shows the localization of the tagged duplex oligonucleotides, 3 or 24 hours after transfection. Tagged oligonucleotides are detected as red dots and the green signal identifies the nuclei of H2B-GFP MCF-7 cells. Enlarged images (bottom images) show that the transfections did result in the localization of the duplex oligonucleotides inside MCF-7 cells both within or outside the nuclei and that the oligonucleotides are still present 24 hours after transfection.

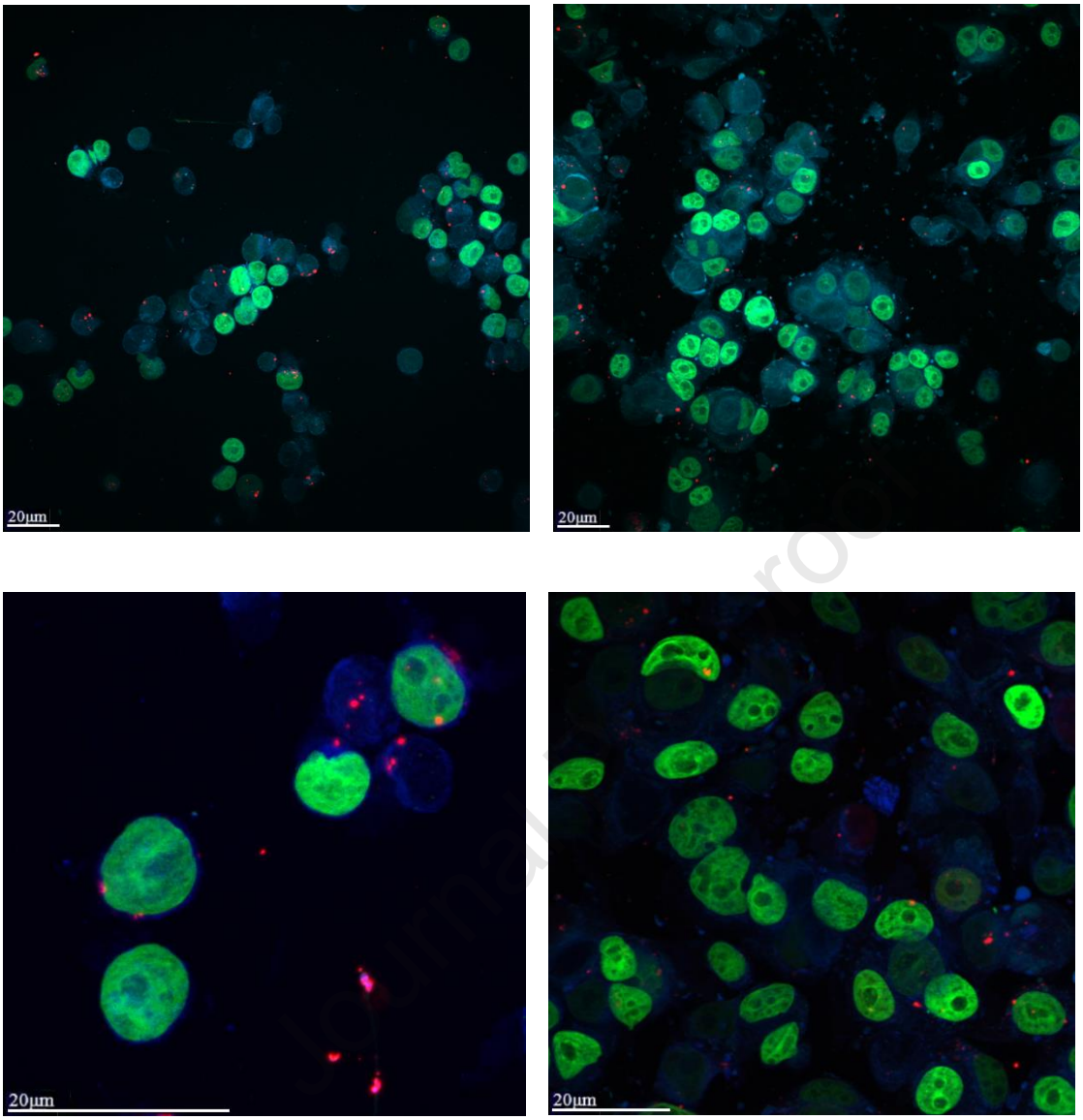

Figure 3: Apotome images showing the localization of the tagged α-ICL in H2B-GFP MCF-7 cells 3 hours after transfection (left) and 24 hours after transfection (right). Top: Composite images, images are maximum intensity projections of three-dimensional image stacks. Bottom: enlarged images (slice). Images show α-ICLs (red dots), MCF-7 nuclei (green signal) and mitochondria (blue dots).

3.2 Changes in MCF-7 and K562 protein expression profiles in response to MC/DMC and ICLs treatments

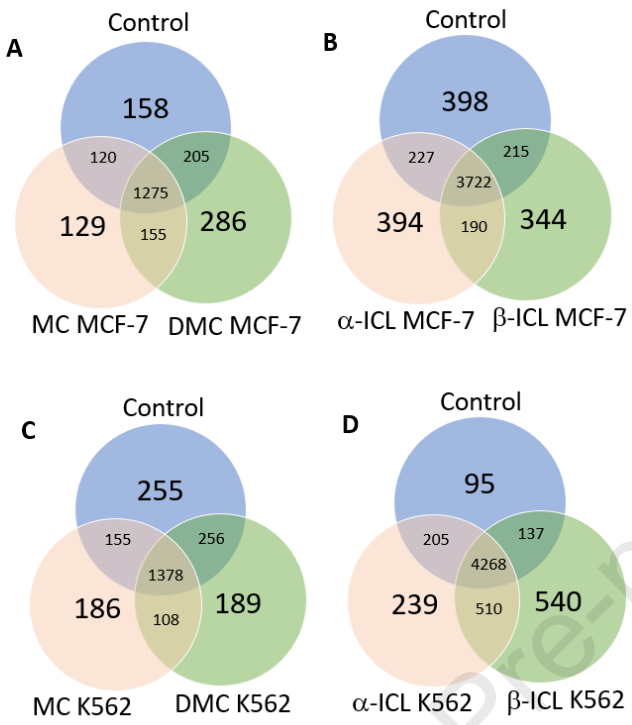

Figure 4: Summary of proteomic changes in MCF-7 and K562 cells in response to MC/DMC and α/β-ICL treatment. Venn diagrams depicting proteins identified in the proteome of MCF-7 and K 562 cells treated by MC/DMC (50 μM) and α/β ICL (10 nM) at 95.0% minimum probability and at least one unique peptide per protein, n=3 replicates for each sample category: control consists of untreated cells (A, C) or cells transfected with duplex DNA without an ICL (B, D). The attained FDR was 2-4% for proteins and 0.14%-2% for peptides. All MS/MS samples were analyzed using PEAKS Studio (Bioinformatics Solutions, Waterloo, ON Canada; version 10.5 and higher). PEAKS Studio was set up to search the reviewed SwissProt database (March 2021; 20385 entries for *Homo sapiens* taxon) as described in detail in the methods section for data analysis.

Figure 4A depicts the Venn diagram from a total of 2328 proteins identified in the proteome of MCF-7 treated with MC, DMC, or untreated cells (control). Results show that 570 proteins are expressed differently upon treatment with MC and/or DMC compared to untreated cells. Among those, 286 proteins are uniquely differently expressed upon DMC treatment, 129 upon MC treatment and 155 by both treatments. Figure 4B depicts the Venn diagram from a total of 5490

proteins identified in the proteome of MCF-7 cells treated with α/β ICL or transfected with a control duplex DNA. Results show that 928 proteins are expressed differently upon treatment with α/β ICL compared to control. Among those, 394 proteins are uniquely differently expressed upon α-ICL treatment, 344 upon β-ICL treatment and 190 by both treatments. Figure 4C shows a total of 2527 proteins identified in the proteome of K562 cells treated with MC/DMC compared to untreated cells. Results show that 483 proteins are differently expressed upon treatment with MC/DMC compared to control. Among those, 186 proteins are uniquely differently expressed upon MC treatment, 189 upon DMC treatment and 108 by both treatments. Figure 4D depicts the Venn diagram from a total of 5994 proteins identified in the proteome of K562 cells treated with α/β ICL. Results show that 1289 proteins are expressed differently upon treatment with α/β ICL compared to control. Among these, 239 proteins are uniquely differently expressed upon α-ICL treatment, 540 upon β-ICL treatment and 510 by both treatments. Full analysis of these proteomic studies will be more thoroughly discussed in a future manuscript.

3.3 Targeted analysis of proteomics results reveals that MC and the α-ICL downregulate the expression of many RAS related proteins in MCF-7 cells while DMC and the β-ICL had a milder effect

Our lab reported previously that MC/DMC could activate $p21^{WAF1/CIP1}$ in MCF-7 (TP53-proficient) and K562 (TP53 mutant) cells in a TP53-independent mode.[17,18] We also discovered that MC/DMC regulate AKT expression in a TP53-dependent manner and that the downregulation of AKT is not associated with the $p21^{WAF1/CIP1}$ activation in response to MC/DMC treatment.[17,18] Since RAS proteins are known players in the upstream mediated signaling and activation of $p21^{WAF1/CIP1}$ which, in turn, controls cell proliferation, we further investigated whether MC/DMC and their corresponding ICLs products could affect the

expression of RAS proteins and impact the regulation of the MAPK/ERK signaling pathways in MCF-7 and K562 cancer cells.

Our global proteomics and LFQ analysis of protein expression profiles show that MC and DMC treatments downregulate the expression of most RAS related proteins compared to control in MCF-7 with MC showing a stronger effect compared to DMC (Figure 5). MC downregulated the expression of 16 out of 21 proteins identified with FDR<4% with 5 protein expressions showing a log2 fold change <-0.5. DMC downregulated the expression of 12 out of 21 proteins identified with FDR<4% with 3 protein expressions showing a log2 fold change <-0.5. The α-ICL downregulated the expression of 17 out of 30 proteins identified with FDR<4% with 2 protein expressions showing a log2 fold change <-0.5 (RAB4B and RAB8A) and 4 showing a log2 fold change >0.5 (RAB14, RAB24, RAP1A, RAB3A). DMC downregulated the expression of 15 out of 30 proteins identified with FDR<4% with 4 protein expressions showing a log2 fold change <-0.5 (RAB4B, RAB8A, RHOT2 and RAP2C) and 2 showing a log2 fold change >0.5 (RAP1A and RAB3A). RAB4B and RAB8A are the most downregulated proteins by both ICLs. These small GTPases are key regulators of intracellular membrane trafficking, from the formation of transport vesicles to their fusion with membranes. Rabs cycle between an inactive GDP-bound form and an active GTP-bound form that is able to recruit to membranes different sets of downstream effectors directly responsible for vesicle formation, movement, tethering and fusion. Interestingly, and of importance for the potential anticancer and antiproliferative effects of ICLs, RAB8A was recently shown to promote breast cancer progression by increasing surface expression of Tropomyosin related kinase B (TrkB).[36] Therefore, the ICLs mediated downregulation of Rab8A may lead to the inhibition of proliferation, migration, and invasion of breast cancer cells by decreasing TrkB surface expression. Our data points to RAB8A as a

potential molecular target of ICLs produced by mitomycins and we propose the prospective usage of ICLs for sensitizing breast tumor cells to additional radiation or chemotherapies.

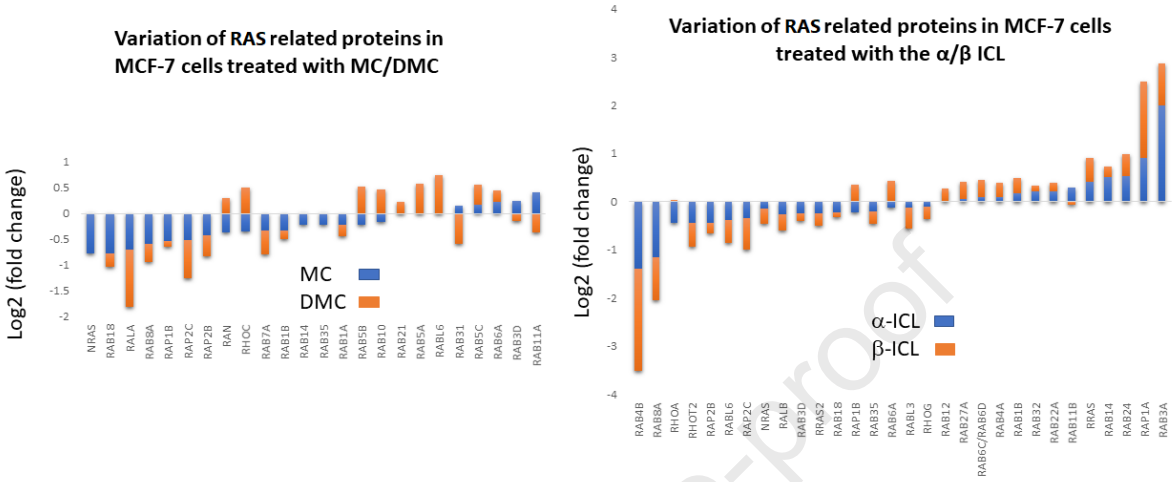

Figure 5: Relative quantitative changes of RAS related proteins in MC/DMC and α/β ICL treated MCF-7 cells. The relative protein abundance profiles were extracted from MS1 areas or MS2 weighted spectra counts in PEAKS X/X+/Pro and Scaffold software respectively, and further processed to calculate the protein fold changes by rescaling their values using a log2 transformation.

The relative quantitative changes in the total (phosphorylated and non-phosphorylated) protein expression of N-RAS, ERK1/2 and pERK/ERK upon MC/DMC treatment and of N-RAS and ERK1/2 upon α/β-ICL treatment were further validated by western blots (Figure 6). We identified a statistically significant ($p<0.05$) downregulation in the expression of N-RAS, ERK1/2 and phospho-ERK1/2 in MCF-7 cells treated with either MC or DMC over a concentration range spanning from 10 to 75 μM (Figure 6 A-C) while the treatment with ICLs induced a mild downregulation of N-RAS but no significant change in ERK1/2 protein expression (Figure 6 D, E).

Moreover, the relative quantitative changes in the expression of N-RAS, ERK1 and ERK2 upon treatment of MCF-7 cells with the α/β ICLs (10 nM for 24 hours at 37°C) were also monitored and quantified using an antibody micro-array (Table 1). In addition to ERK1/2 we chose to analyze the level of ATM expression, a well-known DNA damage sensor marker. ATM is a serine/threonine protein kinase, which activates checkpoint signaling upon double strand breaks (DSBs) and genotoxic stress caused via ionizing UVA light, and potentially, via interstrand crosslinks formation such as the α/β-ICLs presented here.[37]

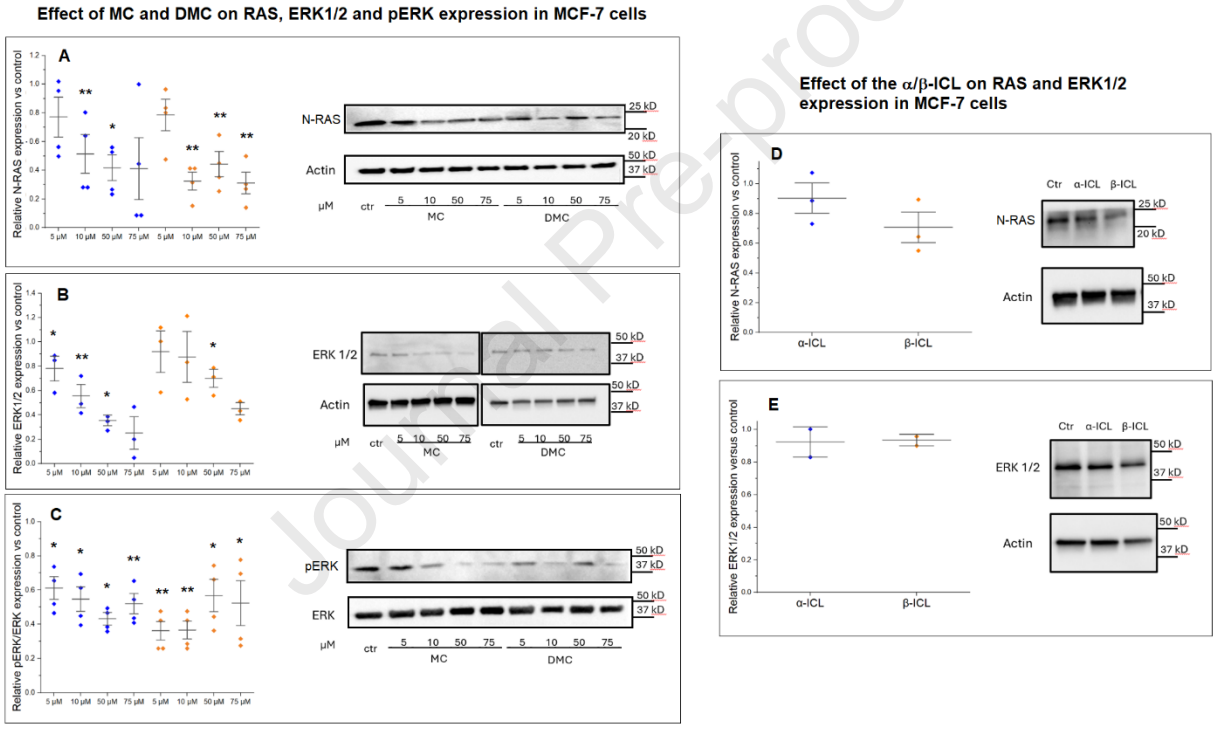

Figure 6: A, B, C: Effects of MC and DMC on N-RAS, ERK1/2 and pERK at various concentrations (5μM to 75μM) in MCF-7 treated cells for 24 hours. The relative phosphorylated ERK levels were detected by western blot analysis with total ERK as the loading control for each sample. The relative phosphorylated ERK levels of controls were taken as 1. Data were collected from at least 3 independent experiments for drug treatment **D, E: Effect of the α/β ICLs on MCF-7 cells when cells were transfected with 10 nM of each ICL for 24 hours**. In the case of ICL treatment, data were collected from at least 3 independent experiments for N-RAS expression and 2 experiments for ERK1/2 expression. (*: $p < 0.05$ vs control and **$p < 0.01$ vs control).

Table 1: Alterations in ERK1, ERK2 and ATM expression quantified by protein array analysis. Total proteins were extracted from MCF-7 cells transfected with 10 nM of each ICL for 24 hours. (data are derived from an average of n=3 biological triplicates).

Fold change (Treatment Sample/Control Sample) in ERK1/2 and ATM protein expression in MCF-7 cells upon α/β-ICL treatment		
	α-ICL	β-ICL
ATM	0.95 (±0.05)	1.10 (±0.13)
ERK 1	1.47 (±0.06)	1.15 (±0.03)
ERK 2	0.81 (±0.04)	0.87 (±0.02)

The data from table 1 suggests that ICL treatment induced a slight decrease in ATM expression in the case of the α-ICL (a 0.95-fold decrease vs control) and a slight increase in the case of the β-ICL (a 1.10-fold increase vs control). In addition, ERK2 was shown to be slightly more downregulated by both ICL than ERK1 which was significantly upregulated by α-ICL treatment (a 1.47-fold increase vs control).

3.4 IPA analysis predicts that the MAPK/ERK pathway is substantially downregulated in MCF-7 by both MC and the α-ICL while DMC and β-ICL have negligible consequences on the same signaling transduction network

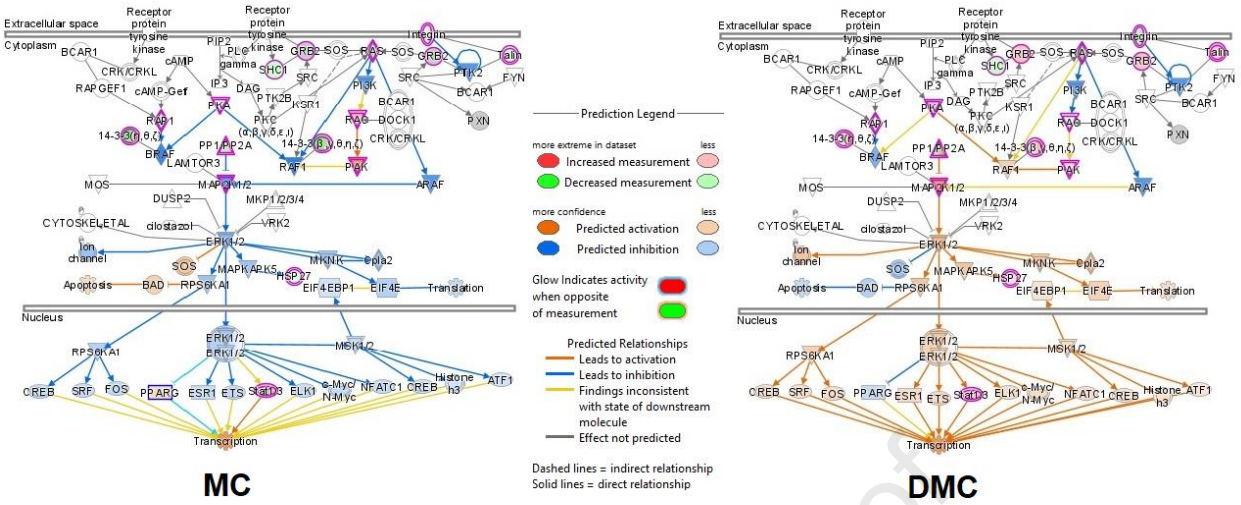

Figure 7: IPA-predicted MAPK/ERK signaling pathway in MCF-7 breast cancer cells showing the MC (A) and DMC (B) mediated quantitative changes in the relative protein abundance profiles as compared with the untreated (control) samples. Protein fold changes are indicated so that fold increases are depicted in red while fold decreases are shown in green. Relative protein abundance profiles predicted by IPA to be inhibited due to their networking relationship with the experimentally identified genes are shown in blue, while the genes that were predicted to be activated are shown in orange.

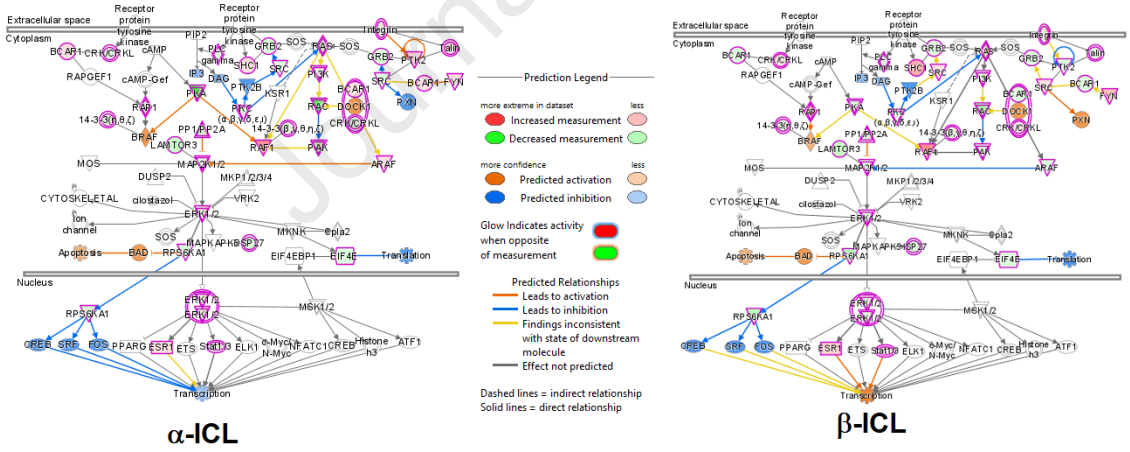

Figure 8: IPA-predicted MAPK/ERK signaling pathway in MCF-7 breast cancer cells showing the α-ICL and β-ICL mediated quantitative changes in the relative protein abundance profiles as compared with the control samples (cells transfected with duplex DNA without an ICL). Protein fold changes are indicated so that fold increases are depicted in red while fold decreases are shown in green. Relative protein abundance profiles predicted by

IPA to be inhibited due to their networking relationship with the experimentally identified genes are shown in blue, while the genes that were predicted to be activated are shown in orange.

We complemented the analysis described in 3.3 with label-free quantitative (LFQ) proteomics profiling to reveal signaling networks that regulate the activation/inhibition of the MAPK/ERK pathway in response to MC/DMC and ICLs treatment. Fold changes upon treatment (MC/DMC and α/β-ICL) in the expression of each quantifiable protein were calculated using the IPA algorithm as described in the methods section. The probability of having a relationship between each IPA indexed biological function and the experimentally determined genes were calculated by a right-tailed Fisher's exact test. The level of significance was set to a p-value of <0.05. Accordingly, the IPA analysis identified the molecular and cellular pathways from the IPA library of canonical pathways that were most significant to the dataset (-log (p value)>2.0). In summary, our bioinformatic analysis (Ingenuity Pathway Analysis) predicted that in the case of MCF-7 cells, both MC/DMC downregulate the MAPK/ERK pathway. IPA assigns a "z score" to all eligible cellular pathways ($z \leq -1.5$ represents significant downregulation while $z \geq 1.5$, significant upregulation). MC was predicted to strongly downregulate this pathway based on the IPA-assigned negative activation z-score (-2.55), whereas DMC was predicted to mildly downregulate the MAPK/ERK pathway (z=-0.21) (Figure 7). In the case of ICL treatment, IPA predicted a different effect for each ICL. The α-ICL was predicted to mildly downregulate the MAPK/ERK pathway (z=-0.24) while the β-ICL was predicted to slightly upregulate it (z=+0.36) (Figure 8). The relative quantitative changes in the expression levels of all molecules quantified by LFQ analysis and IPA-analysis of proteomics data in this pathway are available in the supporting information section of this manuscript (Supporting documents S.2.1 to S.2.4).

3.5 The relative phosphorylation level of many proteins mapped to the JAK/STAT signaling pathway decreases in response to MC and DMC treatment while the p-CREB and p-ERK are the most downregulated proteins mapped to the MAPK/ERK signaling axis in MCF-7 breast cancer cells

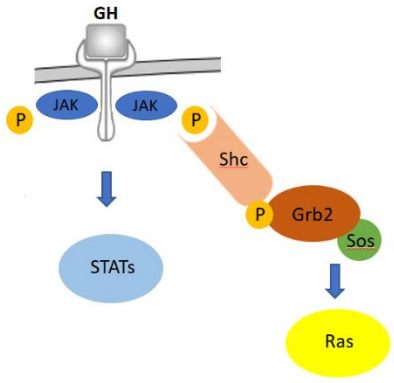

Figure 9: Role of JAK kinases in the upstream component of the MAPK/ERK pathway. Schematic signaling networks showing the crosstalk between the JAK and MAPK/ERK pathways (based on references 27 and 28)

Studies on MAPK/ERK signaling during the last two decades showed that JAK kinases can function as upstream components of at least two signaling pathways that diverge upstream of RAS, one leading to the activation of STATs and the other to activation of MAPK/ERK via the RAS/RAF-1/MEK signaling axis. Most ligands that activate the JAK/STAT pathway were also shown to activate the RAS mediated pathway leading to MAPK/ERK activation (Figure 9).[27,28] We rationalized that a potential decrease in the phosphorylation-induced activation of the JAK/STAT pathway in response to extracellular signals could lead to the decrease in the site-specific phosphorylation of MAPK and ERK with ensuing downregulation of their kinase activity. Accordingly, we further investigated the changes in the level of phosphorylated proteins using phosphoprotein microarray assays in MCF-7 cells (Figure 10). Figure 10 shows that both drugs decreased the level of most phosphorylated proteins in the JAK/STAT pathway, with MC

showing a stronger effect, which correlates with the stronger downregulation of the MAPK/ERK pathway by MC (z=-2.55) compared to DMC (z=-0.21) as predicted by the IPA analyses of LFQ proteomic data presented in Figure 7.

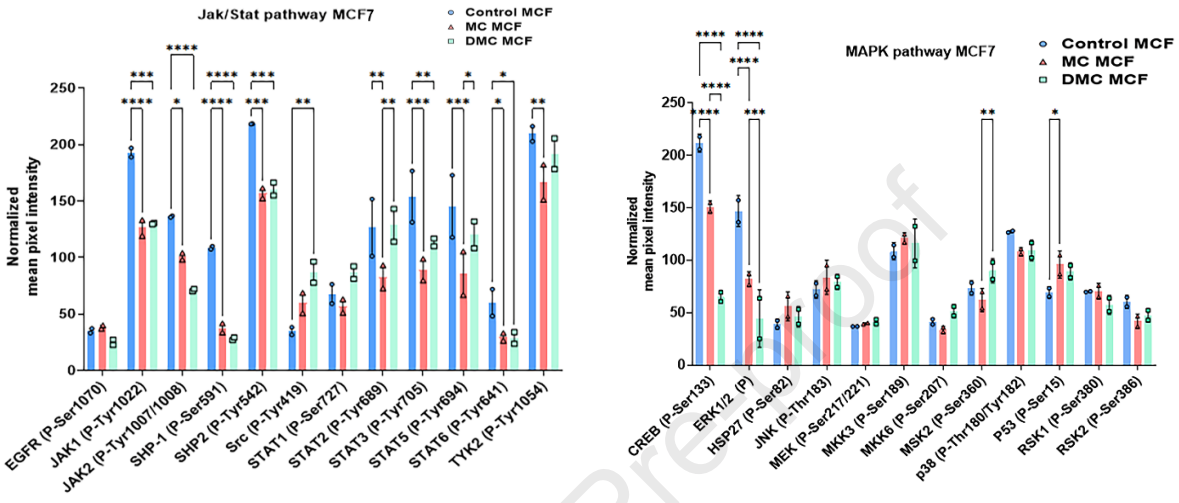

Figure 10: Changes in the level of phosphorylated proteins mapped to the JAK/STAT and MAPK/ERK pathways in MCF-7 cells upon MC/DMC treatment (50 µM for 24 hours). The quantitative changes in the phosphorylation of targeted signaling molecules was performed using the total protein extracts from each MCF-7 treatment and specific mixture of antibodies directed against each investigated phosphosite; the arrays were developed with secondary antibodies coupled with HRP using the protocol from RayBio® C-Series Human Phosphorylation Multi-Pathway Profiling Array C55 (Cat# AAH-PPP-1-8). The quantitative changes in the reported phosphosites were determined from the chemiluminescence readings and calculated as described in the methods sections. The data from phosphoproteomics arrays analysis are presented in Supporting information (Supplementary table S3). Data from the protein arrays were analyzed using the two-way ANOVA followed by multiple comparison tests and Holm-Sidak method. Results were weighted for their statistical significance based on the calculated p-values: $p \leq 0.05$ (*); p<0.01 (**); p<0.001 (***) and p<0.00001 (****).

3.6 Targeted analysis of proteomics results shows that MC/DMC and the α/β-ICL upregulate the expression of most RAS-related proteins in K562 cells but that DMC and the β-ICL show a milder effect

Once we had established the effects of MC/DMC and the α/β-ICLs on RAS related protein expression and had delineated the impact of drug and ICL treatment on the signaling networks within the MAPK/ERK and JAK/STAT pathways in MCF-7 cells (WT TP53), we decided to perform similar analyses with TP53 mutant K562 cells. The targeted LFQ proteomics analysis presented in Figure 11 highlights that MC and DMC treatments, overall, upregulate the expression of many RAS-related oncogenic proteins in K562 cells. Remarkably, MC exhibited a stronger effect as compared to DMC. MC upregulated the expression of 13 proteins out of 20 identified with an FDR<4% with 10 protein expressions showing a log2 fold change >0.5. DMC upregulated the expression of 19 proteins out of 27 proteins identified with FDR<4% with 10 protein expressions showing a log2 fold change >0.5. In contrast, each ICL had a different effect on the expression of RAS-related proteins. The α-ICL upregulated the expression of 21 proteins out of 36 proteins identified with FDR<4% with 7 protein expressions showing a log2 fold change >0.5. The β-ICL downregulated the expression of 23 proteins out of 36 proteins identified with FDR<4% with only 1 protein expression showing a log2 fold change >0.5. For both ICLs, the most downregulated protein is RAB13.[38] Studies point to RAB13 as a key regulator involved in insulin-induced transport to the plasma membrane of the glucose transporter GLUT4; thus, playing a role in glucose homeostasis. As such, the downregulation of Rab13 by both ICLs could induce K562 cancer cell starvation through the impairment in the intracellular import of glucose which could be affected by the decreased numbers of glucose transporters GLUT4. Remarkably our LFQ analysis of other cellular signaling pathways showed that both glycolysis and gluconeogenesis are significantly downregulated in K562 cells treated with either MC or DMC (data to be disclosed in a future manuscript containing detailed LFQ proteomics and statistical analysis of MC vs DMC vs ICLs mediated changes in the protein

expression profiles in K562 in contrast to MCF-7 cancer cells). Moreover, RAB13 is a well characterized tumor promoting signaling molecule for many cancers, including pancreatic, colorectal, stomach, mammary glands, among others (https://www.disgenetplus.com/). Therefore, our data identified RAB13 as a potential molecular target of ICLs produced by mitomycins in leukemia cell lines.

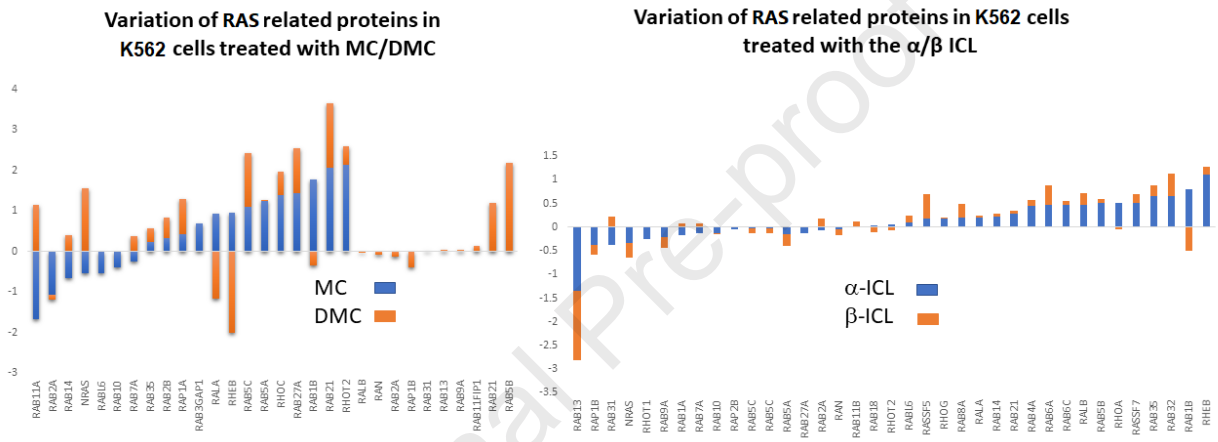

Figure 11: Relative quantitative changes of the level of RAS related proteins in MC/DMC and α/β ICL treated K562 cells. The relative protein abundance profiles were extracted from MS1 areas or MS2 weighted spectra counts in PEAKS X/X+/XPro and Scaffold software respectively, and further processed to calculate the protein fold changes by rescaling their values using a log2 transformation.

The relative quantitative changes in the total (phosphorylated and non-phosphorylated) protein expression of N-RAS, ERK1/2 and pERK/ERK upon MC/DMC treatment and of N-RAS and ERK1/2 upon ICL treatment were further validated by western blots (Figure 12). As in the case of MCF-7 breast cancer cells, we determined the relative quantitative changes in the expression of N-RAS, ERK1 and ERK2 upon treatment of K562 cells with the α/β ICLs (10 nM for 24 hours at 37°C) using an antibody micro-array (Table 2). Similarly, we analyzed the level of expression of ATM. The data presented in Table 2 suggests that α/β-ICLs treatment induced a

slight increase in ATM expression in K562 cells, a very similar effect as the one observed in MCF-7 breast cancer cells when treated with the β-ICL using the same dose and time of exposure (see Table 1). In addition, α/β-ICL treatment resulted in a stronger ERK1 downregulation than in the case of MCF-7 cells. However, only α-ICL treatment resulted in the downregulation of ERK2 in K562 cells.

Table 2: Alterations in ERK1, ERK2 and ATM expression quantified by protein array analysis. Total proteins were extracted from K562 cells transfected with 10 nM of each ICL for 24 hours (data are derived from an average of n=3 biological triplicates).

Fold change (Treatment Sample/Control Sample) in ERK1/2 and ATM protein expression in K562 cells upon α/β-ICL treatment		
	α-ICL	β-ICL
ATM	1.13 (±0.07)	1.12 (±0.04)
ERK 1	0.70 (±0.06)	0.81 (±0.03)
ERK 2	0.69 (±0.03)	1.02 (±0.03)

Additionally, the western blot analysis presented in Figure 12 reveals that the expression of N-RAS showed no significant-change upon treatment with MC/DMC as compared to control and only DMC treatment triggered a modest downregulation of ERK1/2 expression at concentration above 5μM. Both drugs increased the level of p-ERK/ERK significantly at concentrations as low as 5μM with DMC (Figure 12). In contrast, the expression of N-RAS decreased in the presence of α/β ICLs in K562 cell line. The downregulation of N-RAS expression was stronger upon transfection with both ICLs in TP53 mutant K562 cells than in WT T53 MCF-7 cells. The downregulatory effect on ERK1/2 expression upon ICL transfection was modest in each case and in both cell lines.

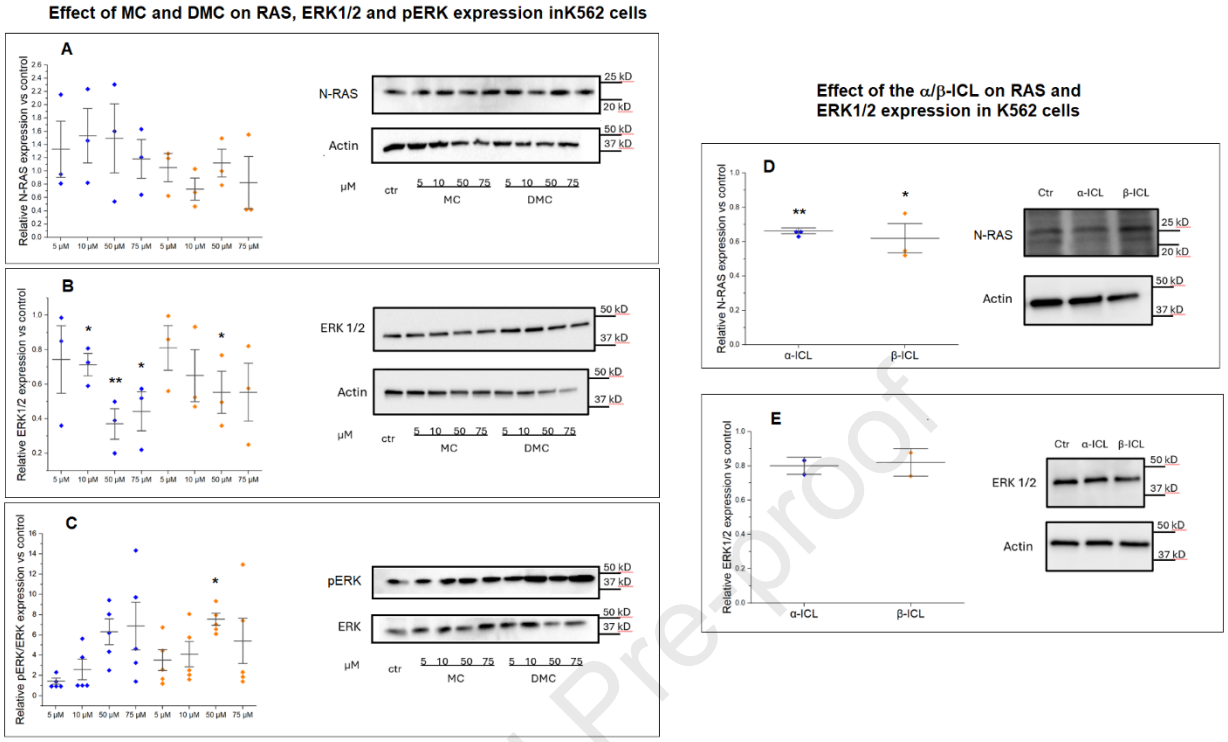

Figure 12 A, B, C: Effects of MC and DMC on N-RAS, ERK1/2 and pERK at various concentrations (5μM to 75 μM) in K562 cells treated cells for 24 hours. The relative phosphorylated ERK levels were detected by western blot analysis with total ERK as the loading control for each sample. The relative phosphorylated ERK levels of controls were taken as 1. Data were collected from at least 3 independent experiments for drug treatment. **D, E: Effect of the α/β-ICLs in K562 cells when cells were transfected with 10 nM of each ICL for 24 hours.** In the case of ICL treatment, data were collected from at least 3 independent experiments for N-RAS expression and 2 experiments for ERK1/2 expression. (*: $p < 0.05$ vs control and **$p < 0.01$ vs control).

3.7 IPA analysis predicts that the MAPK/ERK pathway is modestly upregulated by MC and the α-ICL whereas DMC and the β-ICL mildly downregulate the same signaling network

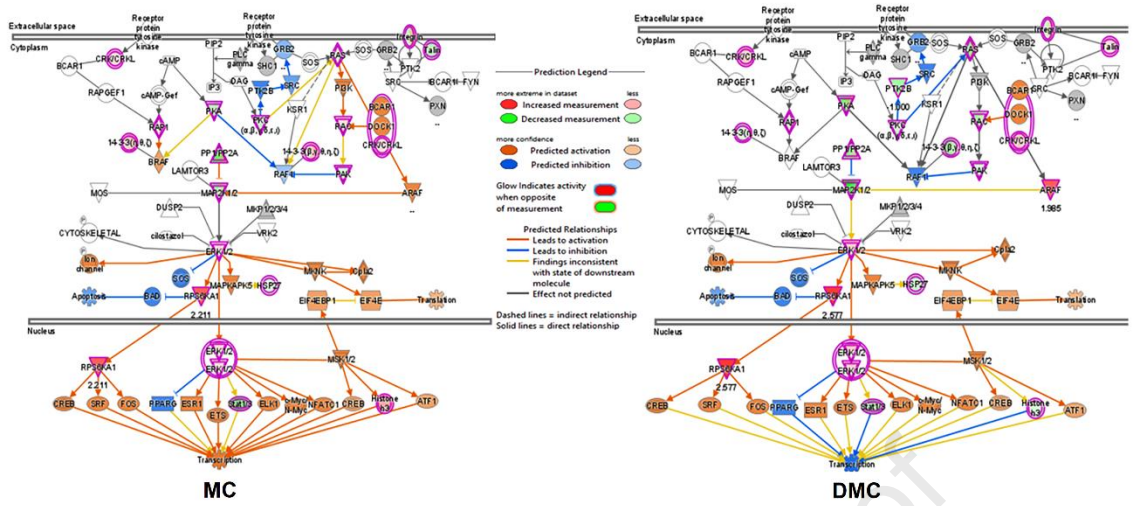

Figure 13: IPA-predicted MAPK/ERK signaling pathway in K562 cells showing the MC (A) and DMC (B) mediated quantitative changes in the relative protein abundance profiles as compared with the untreated (control) samples. Protein fold changes are indicated so that fold increases are depicted in red while fold decreases are shown in green. Relative protein abundance profiles predicted by IPA to be inhibited due to their networking relationship with the experimentally identified genes are shown in blue, while the genes that were predicted to be activated are shown in orange.

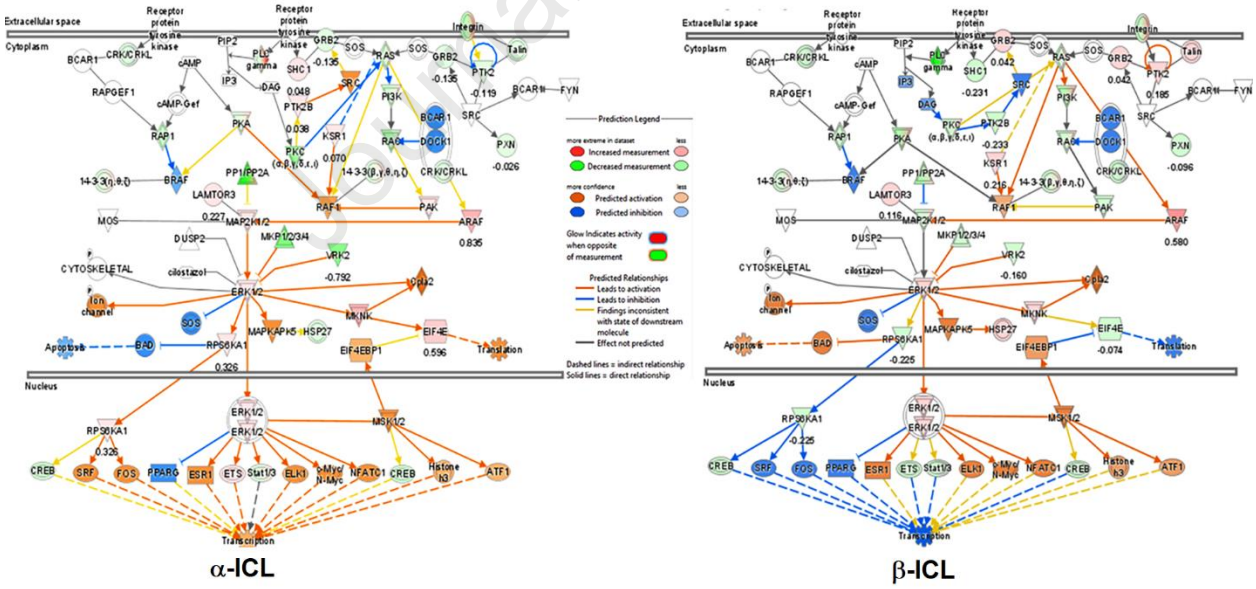

Figure 14: IPA-predicted MAPK/ERK signaling pathway in MCF-7 breast cancer cells showing the α-ICL and β-ICL mediated quantitative changes in the relative protein abundance profiles as compared with the control samples (cells transfected with duplex DNA without an ICL). Protein fold changes are indicated so that fold increases are depicted in

red while fold decreases are shown in green. Relative protein abundance profiles predicted by IPA to be inhibited due to their networking relationship with the experimentally identified genes are shown in blue, while the genes that were predicted to be activated are shown in orange.

We complemented the analysis described in 3.6 with label-free quantitative (LFQ) proteomics profiling to reveal signaling networks regulating the activation/inhibition of the MAPK/ERK pathway in response to MC/DMC and ICLs treatment in K562 cells. This was performed to compare the activation of that pathway in TP53 proficient (MCF-7) vs mutant TP53 (K562) cell lines upon MC/DMC/ICLs treatment (section 3.4 vs 3.7). Fold changes upon treatment (MC/DMC and α/β-ICL) in the expression of each quantifiable protein were calculated using the IPA algorithm as described in the methods section.

In summary, our bioinformatic analysis (Ingenuity Pathway Analysis) of LFQ proteomics data predicts that in the case of K562 cells MC and DMC have opposite effects on the MAPK/ERK pathway activation (Figure 13). MC is predicted to mildly upregulate the MAPK/ERK pathway with an IPA-assigned positive activation z-score (z= +0.56), whereas DMC is predicted to mildly downregulate the MAPK/ERK pathway (z=-1.00) (Figure 12). In the case of ICL treatment, IPA predicts that each ICL effect correlates with that of the drug treatment which produces that ICL. The α-ICL (MC major ICL), like MC, is predicted to mildly upregulate the MAPK/ERK pathway (z=+0.38) while the β-ICL is predicted to slightly downregulate it (z=-0.64) (Figure 14). The relative quantitative changes in the expression levels of all molecules quantified by LFQ analysis and IPA-analysis of proteomics data in this pathway are available in the supporting information section of this manuscript (Supporting documents S.2.5 to S.2.8).

3.8 The phosphorylation level of many proteins mapping to the JAK/STAT and MAPK/ERK signaling pathways are downregulated by MC/DMC in K562 cells with DMC showing a stronger downregulatory effect than MC in MAPK/ERK signaling

The phosphorylation levels of many proteins mapping to the JAK/STAT signaling pathway decreased in response to both MC and DMC treatment (Figure 15). We observed that MC and DMC strongly decreased the level of all but 2 phosphoproteins in that pathway (EGFR and SHP2). Moreover, MC/DMC treatment led to a stronger downregulatory effect on p-STAT2,3,5 in K562 cells than in the case of MCF-7 cells. DMC showed a stronger downregulatory effect on p-MEK, p-P38 and mutant p-P53 expression in proteins mapped to the MAPK/ERK signaling axis in K562 cells. This correlates with the stronger downregulation (z=-1.00) of the MAPK/ERK pathway observed upon DMC treatment versus MC treatment in K562 cells.

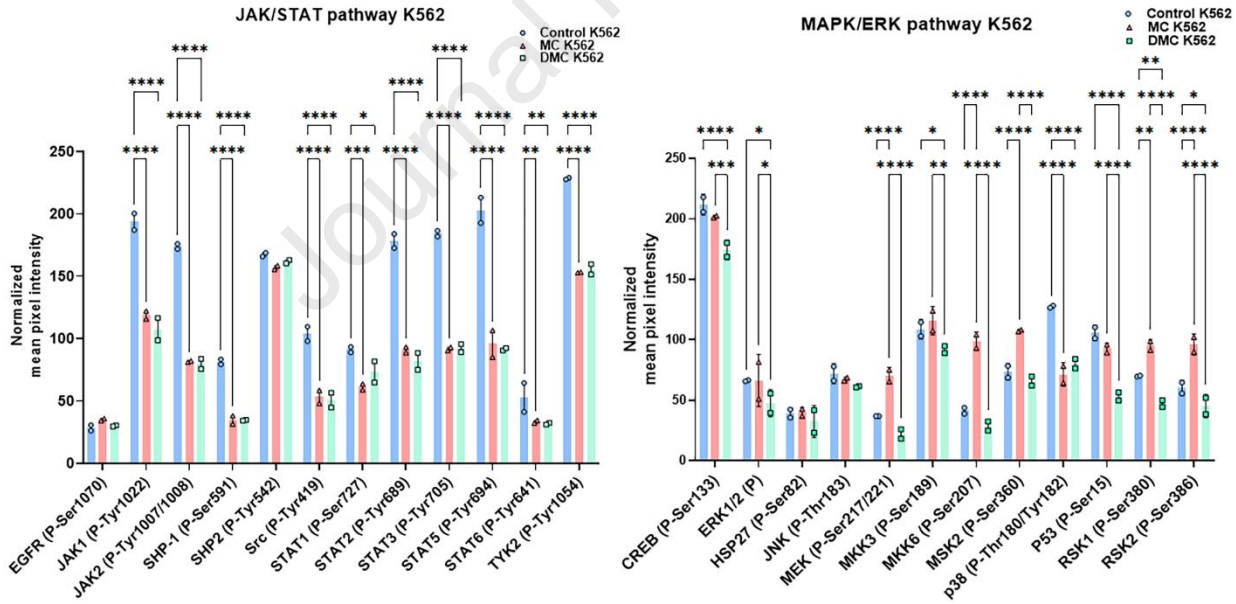

Figure 15: Changes in the level of phosphorylated proteins in the MAPK/ERK and JAK/STAT pathway in K562 cells upon MC/DMC treatment (50µM for 24 hours). The quantitative changes in the phosphorylation of targeted signaling molecules was performed using the total protein extracts from each K562 treated condition and specific mixture of antibodies directed against each investigated phosphosite; the arrays were developed with secondary

antibodies coupled with HRP using the protocol from RayBio® C-Series Human Phosphorylation Multi-Pathway Profiling Array C55 (Cat# AAH-PPP-1-8). The quantitative changes in the reported phosphosites were determined from the chemiluminescence readings and calculated as described in the methods sections. The data from phosphoproteomics arrays analysis are presented in the supporting information section (Supplementary Table 3). Data from the protein arrays were analyzed using the two-way ANOVA followed by multiple comparison tests and Holm–Sidak method. Results were weighted for their statistical significance based on the calculated p-values: $p \leq 0.05$ (*); $p<0.01$ (**); $p<0.001$ (***) and $p<0.00001$ (****).

4. DISCUSSION

4.1 Effect of MC/DMC and α/β-ICLs on MAPK/ERK pathway in WT P53 MCF-7 cell line

Table 3: Summary of the effect of MC/DMC and α/β-ICLs on RAS related oncogenic proteins and MAPK/ERK pathway activation in MCF-7 and K562 cells.

Cell line	MCF-7				K562			
Treatment	MC	α-ICL	DMC	β-ICL	MC	α-ICL	DMC	β-ICL
RAS related proteins	↓	↓	↓	=	↑	↑	↑	↓
MAPK/ERK pathway	z:-2.55 ↓	z:-0.24 ↓	z:-0.21 ↓	z: 0.36 ↑	z: 0.56 ↑	z: 0.38 ↑	z:-1.00 ↓	z:-0.64 ↓
N-RAS	↓	↓	↓	↓	=	↓	↓	↓
ERK1/2	↓	ERK1 ↑ ERK2 ↓	↓	ERK1 ↑ ERK2 ↓	↓	ERK1 ↓ ERK2 ↓	↓	ERK1 ↓ ERK2 =
pERK/ERK	↓	NA	↓	NA	↑	NA	↑	NA

The research presented herein is the first to show the effects of two mitomycins, MC and DMC, on the regulation of RAS related proteins and on the activation of the MAPK/ERK pathway in MCF-7 cell lines. Table 3 summarizes our findings. Overall MC and DMC were both efficient

in decreasing the relative abundance of both RAS and RAS related proteins as well as ERK1/2 and phospho-ERK1/2 proteins. Accordingly, the bioinformatics analysis performed from our proteomic profiling data predicts that MC and DMC both downregulate the MAPK/ERK signaling pathway with MC showing a stronger downregulatory effect. Both drugs form stereoisomeric ICLs in mammalian cells called α-ICL (*trans*) and β-ICL (*cis*), respectively and the current scientific paradigm is that these ICLs are primarily responsible for the cytotoxicity of mitomycins. However, since mitomycins also generate other types of adducts (DNA monoadducts and protein adducts), the exact role of each ICL and of its structure in the toxicity of these compounds is not well understood. We designed an assay whereby a double-stranded oligonucleotide bearing a single ICL at a specific site is transfected into cells. After transfection, protein lysates are used to pinpoint the effect of each ICL on protein expression. Our data show that both ICLs triggered the downregulation of N-RAS proteins with the β-ICL showing a stronger downregulatory effect than the α-ICL. The effect on total ERK expression was small and similar for both ICLs and our results suggest that ERK2 expression is more impacted by both ICLs than ERK1 expression. In addition, bioinformatics analysis predicts that each ICL has a different effect on the MAPK/ERK signaling pathway: while the α-ICL is predicted to downregulate the MAPK/ERK pathway, the β-ICL is predicted to upregulate that same pathway. Overall results suggest that the MAPK/ERK pathway in MCF-7 cells is more strongly downregulated by MC and the α-ICL than by DMC and the β-ICL suggesting that the structure of DNA lesions formed by mitomycins is relevant to the impact of the drug on the RAS signaling pathway activation in MCF-7 cells. Changes in the level of phosphorylated proteins mapped in the MAPK/ERK pathway in MCF-7 cells upon MC/DMC treatment show that p-CREB (Ser 133) is the most downregulated phosphoprotein. In canonical CREB signaling, CREB becomes activated through phosphorylation of Serine 133 in response to

the cAMP-dependent protein kinase A (PKA) pathway and plays a central position orchestrating cell survival, growth, and differentiation.[39] Our results show that this downregulation is more pronounced upon DMC treatment, therefore, this downregulation may be a major mechanism through which DMC impacts MCF-7 cell proliferation.

4.2 Effect of MC/DMC and α/β ICLs on RAS and ERK1/2 expression in TP53 mutant K562 leukemia cell line

MC and DMC did not have any effect on the expression of N-RAS in TP53 mutant K562 cells although both the corresponding ICLs products of each drug were capable of downregulating N-RAS expression. MC and DMC as well as both ICLs slightly downregulated ERK1/2 expression. Surprisingly, the phosphorylated level of ERK proteins increased upon MC/DMC treatment. Overall, the bioinformatics analysis of our LFQ proteomic profiling data predicts that both MC and the α-ICL upregulate the MAPK/ERK signaling pathway whereas DMC and the β-ICL show a downregulatory effect. In summary, these findings suggest that in TP53 mutant K562 cells the stereochemical configuration of the major ICL produced by each drug is a determinant factor contributing to the differential regulation of the MAPK/ERK pathway.

The noticeable effects of MC and DMC on the MAPK/ERK pathway in K562 cells were further evidenced by changes in the level of phosphorylated proteins mapped to this pathway. Figure 15 shows that phosphoprotein p-CREB (Ser 133), p-MEK (Ser 217/221), p-P38 (Thr 180/Tyr 182), p-RSK1 (Ser 380) and mutant p-P53 are all downregulated upon DMC treatment. In contrast, MC treatment triggered an increase in the expression of p-MEK (Ser 217/221), p-MKK6 (Ser 207), p-RSK1 (Ser 380) and p-RSK2 (Ser 386). These results correlate with the regulation of the MAPK/ERK pathway by MC/DMC identified through bioinformatics analysis of our LFQ proteomics data. Relevant to our previous study on MC/DMC impact on $p21^{WAF1/CIP1}$

expression, it should be noted that p38, which is strongly affected by MC/DMC treatment, plays a major role in the negative regulation of cell cycle progression at both G1/S and G2/M transition through the upregulation of CDK inhibitors.[40]

4.3 Effect of MC/DMC on phosphoproteins mapped in the canonical JAK/STAT pathway.

Most phosphoproteins in the JAK/STAT canonical pathway are downregulated upon MC/DMC treatment in MCF-7 and K562 cell lines. MC shows a stronger downregulating effect in MCF-7 than DMC, whereas the effect of both drugs is similar in K562 cells. The most downregulated phosphoproteins in this pathway are p-JAK1, p-JAK2, p-SHP1 and the phospho-STATs proteins. JAK1 plays a crucial role in effecting the expression of proteins that mediate inflammation, epithelial remodeling and metastatic cancer progression. JAK2 is essential for growth factor signaling which is also regulated by SHP1.[41,42] STATs proteins are transcription factors which also mediate cellular proliferation and apoptosis. Our results suggest that MC/DMC impact on phosphoprotein expression mapped in the JAK/STAT pathway contribute to the anti-proliferation effect observed in MCF-7 and K562 cells upon drug treatment.

The JAK/STAT canonical pathway is known to signal upstream of the MAPK/ERK pathway. In MCF-7 cells, both pathways are downregulated by MC/DMC treatment. The same correlation is observed in TP-53 mutant K562 cells upon DMC treatment whereas, with MC, the downregulation of the JAK/STAT pathway contrasts with the upregulation of the MAPK/ERK pathway. Indeed, both MC and the α-ICL are shown to upregulate MAPK/ERK. This highlights the complexity of cellular mechanisms which are fine-tuned by multiple, cross-talking pathways.

4.4 Potential upstream signaling of $p21^{WAF1/CIP1}$ activation in the control of cell proliferation and cell death by mitomycins

Our investigation on the impact of MC/DMC on RAS signaling stems from our interest in determining the upstream signaling of $p21^{WAF1/CIP1}$ activation in the control of cell proliferation and cell death by mitomycins in cells with or without a functional TP53. We previously showed that both MC/DMC activate p21 in MCF-7 cells (WT TP53) and K562 cells (mutant TP53) in a p53-independent mode,[17] however, the upstream signaling of $p21^{WAF1/CIP1}$ remains unidentified. TP53-independent $p21^{WAF1/CIP1}$ transcription has been reported by several RAS-related transcription factors, depending on the cell line and the cellular context: ELK-1 in sodium arsenite-exposed human keratinocyte HaCaT cells,[43] C/EBP and Ets transcription factors in MAPK-activated human hepatocarcinoma HepG2 cells,[44] TAT1 and 3 in IL-6 stimulated osteosarcoma MG63 cells[45] and Forkhead Box O transcription factors in response to Raf/MEK and JNK activation in B-RafV600E melanoma cells.[46] Moreover and relevant to this study, research by others showed that Sp1 may replace TP53 to mediate $p21^{WAF1/CIP1}$ transcription in Raf/MEK/ERK-activated cancer cells with a mutated TP53 (U251, LNCaP and SK-MEL28) and that Sp1 requirement in Raf/MEK/ERK-induced $p21^{WAF1/CIP1}$ transcription is subject to TP53 status.[47] Our results here show that in the case of TP53 mutant cells K562 and in contrast to TP53 proficient MCF-7 cells, pERK/ERK expression increases in response to the MC/DMC treatment. This activation of ERK may also be involved in the regulation of $p21^{WAF1/CIP1}$ activation although the molecular mechanism through which this might occur remains to be elucidated. It will be particularly interesting to investigate the role of Sp1 in $p21^{WAF1/CIP1}$ transcription in K562 cells upon treatment with MC/DMC.

Apart from direct transcription, $p21^{WAF1/CIP1}$ activation is also modulated through phosphorylation. At least 7 phosphorylation sites (Thr57, Ser130, Thr145, Ser146, Ser14, Ser153 and Ser160), targeted by a diversity of distinct kinases, play a role in the regulation of $p21^{WAF1/CIP1}$.[48] We have previously investigated the phosphorylation of $p21^{WAF1/CIP1}$ at Thr145 and Ser146 in MCF-7 and K562 upon MC/DMC treatments, which affects p21/PCNA binding as well as regulates $p21^{WAF1/CIP1}$ interplay with its associated proteins, its localization and stability. We found that MC/DMC treatment triggered $p21^{WAF1/CIP1}$ activation in both cell lines through a decreased level of relative phosphorylation at Thr145.[17] This results in the nuclear localization of $p21^{WAF1/CIP1}$ and the ability for $p21^{WAF1/CIP1}$ to interact with PCNA. We found that the deactivation of AKT, a main kinase able to phosphorylate $p21^{CIP1}$, occurs in MCF-7 cells, but not in K562 cells upon MC/DMC treatment. However, this deactivation of AKT by MC and DMC is p53-dependent and therefore, is not responsible for the TP53 independent activation of $p21^{WAF1/CIP1}$ in MCF-7 cells (WT TP53) and K562 cells (mutant TP53).[18]

Pim-1[49], PKA[50], and PKC[48] are other kinases able to phosphorylate $p21^{WAF1/CIP1}$ at Thr 145. Therefore, the potential regulation of the TP53-independent phosphorylation of $p21^{WAF1/CIP1}$ observed in MCF-7 and K562 upon MC/DMC treatment warrants further investigation.

5. Conclusion

Our results on the effect of MC/DMC on RAS signaling opens several avenues for research: 1) one possibility is that crosstalk between the RAS pathway and transcriptional regulation of genes encoding proteins of the downstream branch of the cAMP-PKA pathway may be involved in the regulation of $p21^{WAF1/CIP1}$ phosphorylation since the level of PKA expression is impacted by MC/DMC treatment in MCF-7 cells (Figure 7) and K562 cells (Figure 12)[51] 2) It would also be interesting to monitor the phosphorylation of $p21^{WAF1/CIP1}$ at Thr57 and Ser130 of

$p21^{WAF1/CIP1}$ since these sites are specific phosphorylation sites for ERK2 and since the expression of ERK2 seems to be more impacted by the ICLs than ERK1 in both cell lines.[52] Data from the literature also indicates that ATM, whose expression is mildly impacted by both ICLs in both cells lines, can activate ERK and mediate cell cycle arrest in a p53-independent manner.[53] 3) $p21^{WAF1/CIP1}$ activation can also be modulated by phosphorylation at Ser146. We previously found that only DMC was able to induce $p21^{WAF1/CIP1}$ dephosphorylation at Ser146 in K562 cells albeit at a high concentration. One possibility is that PKC or RSK 2, downstream effector targeted by ERK1/2, can phosphorylate $p21^{WAF1/CIP1}$ at Ser146 upon DMC treatment in K562 cells.[54] 4) Previous studies also showed that $p21^{WAF1/CIP1}$ can be phosphorylated by the Pim-1 kinase. Since Pim-1 transcription is initiated by STAT3 and STAT5, and since both MC and DMC decrease the level of phosphorylated of STAT3/5 in both cell lines, it would be relevant to investigate if the drugs effect on STAT3/5 phosphorylation status leads to a decrease in pim1 protein expression that could further affect $p21^{WAF1/CIP1}$ phosphorylation level.[55]

So far, our hypothesis is that DNA ICLs formed by MC/DMC are responsible for events leading to the TP53-independent changes in the $p21^{WAF1/CIP1}$ protein expression/phosphorylation detected in MCF-7 and K562 cancer cells. This proposed molecular mechanism of action was backed up by the fact the α-ICL itself was enough to cause $p21^{WAF1/CIP1}$ activation and regulation of AKT phosphorylation in MCF-7 cells.[17,18] Results reported herein show that RAS expression is downregulated by both ICLs in both MCF-7 and K562 cell lines. However, one alternative explanation is that ROS produced by MC/DMC treatments induce several redox-dependent changes in cell cycle-related proteins. One of these is the p53-independent accumulation of $p21^{WAF1/CIP1}$, which requires the integrity of the RAS-MAPK pathway.[56] This alternate mechanism may also be responsible for MC/DMC impact on p21 activation.

Finally, this study has identified two potential molecular targets of mitomycin ICLs: RAB8A, which was recently shown to promote breast cancer progression, was strongly downregulated by both ICLs in breast tumor cells MCF-7 whereas RAB13, an oncogenic driver for many cancers, was strongly downregulated by both ICLs in leukemia K562 cells. These findings open therapeutic avenues for the prospective usage of ICLs to sensitize tumor cells to additional radiation or chemotherapies.

ACKNOWLDEGEMENTS This study was supported by the National Institute of Health [grants numbers 1R16GM149514-01 and 2SC3GM105460-S1, S2, S3 to E.C] and was supported by the PRISM program at John Jay College of Criminal Justice. PRISM is the Program for Research Initiatives for Science Majors at John Jay College and funded by the Title V, HSI-STEM and MSEIP programs within the U.S. Department of Education; the PAESMEM program through the National Science Foundation; and New York State's Graduate Research and Teaching Initiative.

CONFLICT OF INTEREST The authors declare that they have no conflict of interest.

References

1. Hata T., Hoshi T., Kanamori K., Matsumae A., Sano Y., Shima T. and Sugawara R. Mitomicin, a new antibiotic from Streptomyces. *I. J. Antibiot.*, Ser.A*9*. 1956: 141-146. PMID: 13385186.
2. Bradner W. T. Mitomycin C: A clinical update. *Cancer Treat. Rev.* 2001; (27): 35-50. doi: 10.1053/ctrv.2000.0202. PMID: 11237776.
3. Verweij J. and Pinedo, H. Cancer chemotherapy and biological modifiers. In Pinedo H.M., Chabner B.A., Longo. D.L. (eds), *Annual 11*. Elsevier Science Publishers B.V., Amsterdam, 1990 p. 67.
4. Chabner B.A., Amrein P.C., Druker B.J., Michaelson M.D., Mitsiades C.S., Goos P.E., Ryan D.P., Ramachandra S., Richardson P.J., Supko J. G. and WilsonW. H. Antineoplastic agents. In Brunton L.L., Lazo J.S., Parker K.L. (eds), *Goodman & Gilman's The Pharmalogical Basis of Therapeutics.* McGraw-Hill Publishers, New York, 2005 pp. 1315-1403.
5. Shannon N.B., Tan J. W.-S., Tan H. L., Wang W., Chen Y., Lim H. J., Tan Q. X., Hendrikson J., Ng W. H., Loo L. Y., Skantakumar T., Wasudevan S. D., Kon O. L., Lim T. K. H., Tan G. H. C., Chia C. S., Soo K. C., Ong C-A J and Teo M. C. C. A set of molecular markers predicts chemosensitivity to Mitomycin-C following cytoreductive surgery and hyperthermic intraperitoneal chemotherapy for colorectal peritoneal metastasis. *Sci. Rep.* 2019; (9): 10572. doi: 10.1038/s41598-019-46819-z. PMID: 31332257; PMCID: PMC6646658.
6. Paz M.M. and Pritsos C.A. The Molecular toxicology of mitomycin C. In Fishbein, J.C. (ed), *Advances in Molecular Toxicology Vol 6*. Elsevier Science Publishers B.V., Amsterdam, 2012 pp. 244-286.

7. Bass P. D., Gubler D.A., Judd T.C. and Williams R.M. Mitomycinoid alkaloids: mechanism of action, biosynthesis, total syntheses, and synthetic approaches. *Chem. Rev.* 2013; (113): 6816-6863. doi: 10.1021/cr3001059. Epub 2013 May 8. PMID: 23654296; PMCID: PMC3864988.

8. Tomasz M. Mitomycin C: small, fast and deadly (but very selective) *Chem. Biol.* 1995; (2): 575-579. doi: 10.1016/1074-5521(95)90120-5. PMID: 9383461.

9. Lawley P.D. and Phillips D.H. DNA adducts from chemotherapeutic agents. *Mutat. Res.* 1996; (355): 13-40. doi: 10.1016/0027-5107(96)00020-6. PMID: 8781575.

10. Palom Y., Suresh Kumar G., Tang L.Q., Paz M.M., Musser S.M., Rockwell S. and Tomasz M. Relative toxicities of DNA cross-links and monoadducts: New insights from studies of decarbamoyl mitomycin C and mitomycin C. *Chem. Res. Toxicol.* 2002; (15): 1398-1406. doi: 10.1021/tx020044g. PMID: 12437330.

11. Aguilar W., Paz M. M., Vargas A., Cheng S.-Y., Clement C.C. and Champeil E. Sequence-dependent diastereospecific and diastereodivergent crosslinking of DNA by decarbamoylmitomycin C. *Chem. Eur. J.* 2018; (24): 6030-6035. doi: 10.1002/chem.201705771. PMID: 29504661; PMCID: PMC7046179.

12. Paz M.M., Ladwa S., Champeil E., Liu Y., Rockwell S., Boamah E. K., Bargonetti J., Callahan J., Roach J. and Tomasz M. Mapping DNA adducts of mitomycin C and decarbamoyl mitomycin C in cell lines using liquid chromatography/electrospray tandem mass spectrometry. *Chem. Res. Toxicol.* 2008; (21): 2370-2378. doi: 10.1021/tx8002615. PMID: 19053323; PMCID: PMC2630229.

13. Xiao G., Kue P., Bhosle R. and Bargonetti, J. Decarbamoyl mitomycin C (DMC) activates p53-independent ataxia telangiectasia and rad3 related protein (ATR) chromatin eviction. *Cell Cycle* 2015; (14): 744-754. doi: 10.1080/15384101.2014.997517. PMID: 25565400; PMCID: PMC4418290.

14. Boamah E.K., White D.E., Talbott K.E., Arva N. C., Berman D., Tomasz M. and Bargonetti J. Mitomycin DNA adducts induce p-53 dependent and p-53 independent cell death pathways. *ACS Chem. Biol.* 2007 (2): 399-407. doi: 10.1021/cb700060t. Epub 2007 May 25. PMID: 17530733; PMCID: PMC2886584.

15. Boamah E. K., Breckman A., Tomasz M., Myeku N., Figueiredo-Pereira M., Hunter S., Meyer J., Bhosle R.C. and Bargonetti J. DNA adducts of decarbamoyl mitomycin C efficiently kill cells without wild-type p53 resulting from proteasome-mediated degradation of checkpoint protein 1. *Chem. Res. Toxicol.* 2010; (23): 1151-1162. doi: 10.1021/tx900420k. PMID: 20536192; PMCID: PMC2907727.

16. Bargonetti J., Champeil E. and Tomasz, M. Differential toxicity of DNA adducts of mitomycin C. *J. Nucleic Acids* 2010; 1-6, e 698960. doi: 10.4061/2010/698960. PMID: 20798760; PMCID: PMC2925095.

17. Cheng S.-Y., Seo J., Huang B. T., Napolitano T. and Champeil E. Mitomycin C and decarbamoyl mitomycin C induce p53-independent p21 activation *Int. J. Oncol.* 2016; (49): 1815-1824. doi: 10.3892/ijo.2016.3703. Epub 2016 Sep 23. PMID: 27666201; PMCID: PMC5063421.

18. Cheng S.-Y., Vargas J, Lee J.-Y., Clement C.C. and Champeil E. Involvement of Akt in mitomycin C and its analog triggered cytotoxicity in MCF-7 and K562 cancer cells. *Chem. Biol. Drug Des.* 2018; (92): 2023-2034. doi: 10.1111/cbdd.13374. Epub 2018 Sep 11. PMID: 30091208; PMCID: PMC6251731.

19. Cheng S.-Y., Delgado-Cruzata L., Clement C. C., Zacarias O., Concheiro-Guisan M., Towler N., Snyder T., Zheng M., Almodovar N., Gonzalez C., Romaine M., Sapse A.-M. and Champeil E.

Cytotoxicity, crosslinking and biological activity of three mitomycins, *Bioorganic Chemistry* 2022; (123): 105744-105761. doi: 10.1016/j.bioorg.2022.105744. PMID: 35349830; PMCID: PMC9050950.

20. Simanshu D. K., Nissley D. V. and McCormick F. RAS proteins and their regulators in human disease. *Cell* 2017; (170): 17-33. doi: 10.1016/j.cell.2017.06.009. PMID: 28666118; PMCID: PMC5555610.

21. Malumbres M. and Barbacid M. RAS oncogenes: the first 30 years. *Nat. Rev. Cancer* 2003; (3): 459-465. doi: 10.1038/nrc1097. Erratum in: Nat Rev Cancer. 2003 Sep;3(9):708. PMID: 12778136.

22. Pylayeva-Gupta Y., Grabocka E. and Bar-Sagi D. RAS oncogenes: weaving a tumorigenic web. *Nat. Rev. Cancer* 2011; (11): 761-774. doi: 10.1038/nrc3106. PMID: 21993244; PMCID: PMC3632399.

23. Drosten M., Dhawahir A., Sum E. Y. Urosevic J., Lechuga C. G., Esteban L. M., Castellano E., Guerra C., Santos E. and Barbacid M. Genetic analysis of Ras signalling pathways in cell proliferation, migration, and survival. *EMBO J.* 2010; (29): 1091-1104. doi: 10.1038/emboj.2010.7. Epub 2010 Feb 11. PMID: 20150892; PMCID: PMC2845279.

24. Drosten M., Lechuga. C. G. and Barbacid M. Ras signaling is essential for skin development. *Oncogene* 2014; (33):2857-2865. doi: 10.1038/onc.2013.254. Epub 2013 Jul 8. PMID: 23831572.

25. Drosten M., Sum E. Y., Lechuga C. G., Simón-Carrasco L., Jacob H. K., García- Medina R., Huang S., Beijersbergen R., Bernards R. and Barbacid M. Loss of p53 induces cell proliferation via Ras-independent activation of the Raf/Mek/Erk signaling pathway. *Proc. Natl. Acad. Sci. USA* 2014; (111): 15155-15160. doi: 10.1073/pnas.1417549111. Epub 2014 Oct 6. PMID: 25288756; PMCID: PMC4210339.

26. Hwang C.Y., Lee C. and Kwon K.S. Extracellular signal-regulated kinase 2-dependent phosphorylation induces cytoplasmic localization and degradation of p21Cip1. *Mol Cell Biol.* 2009; (12): 3379-3389. doi: 10.1128/MCB.01758-08. PMID: 19364816; PMCID: PMC2698740.

27. Winston L.A. and Hunter T. Intracellular signalling: putting JAKs on the kinase MAP. *Curr Biol.* 1996 (6):668-671. doi: 10.1016/s0960-9822(09)00445-x. PMID: 8793290.

28. Jha A., Alam M., Kashyap T., Nath N., Kumari A., Pramanik K.K., Nagini S. and Mishra R. Crosstalk between PD-L1 and Jak2-Stat3/ MAPK-AP1 signaling promotes oral cancer progression, invasion and therapy resistance. *Int Immunopharmacol*. 2023 (124,Pt A):110894. doi: 10.1016/j.intimp.2023.110894. Epub 2023 Sep 6. PMID: 37678027.

29. Kinoshita S., Uzu K., Nakano K. and Takahashi,T. Mitomycin derivatives. 2. Derivatives of decarbamoylmitosane and decarbamoylmitosene. *J. Med. Chem.*, 1971; (14): 109-112. doi: 10.1021/jm00284a006.

30. Clement C.C., Aphkhazava D., Nieves E., Callaway M., Olszewski W., Rotzschke O. and L. Santambrogio. Protein expression profiles of human lymph and plasma mapped by 2D-DIGE and 1D SDS-PAGE coupled with nanoLC-ESI-MS/MS bottom-up proteomics. *J Proteomics*, 2013; (78): 172-187. doi: 10.1016/j.jprot.2012.11.013. PMID: 23202415; PMCID: PMC3631612.

31. Clement C.C., Moncrieffe H., Lele A., Janow G., Becerra A., Bauli F., Saad F.A., Perino G., Montagna C., Cobelli N., Hardin J., Stern L.J., Ilowite N., Porcelli S.A., and Santambrogio L Autoimmune response to transthyretin in juvenile idiopathic arthritis. *JCI Insight*, 2016; (2): e85633. doi: 10.1172/jci.insight.85633. PMID: 26973882; PMCID: PMC4784708.

32. Zacarias O., Petrovic A. G., Abzalimov R., Pradhan P. and Champeil E. Synthesis of oligonucleotides containing *trans* mitomycin C-DNA adducts at N^6 of adenine and N^2 of guanine. *Chem. Eur. J., 2021;* (57): 14263-14272. doi: 10.1002/chem.202102338. PMID: 34319608; PMCID: PMC8516704.
33. Aguilar W., Zacarias O., Romaine M., Proni G., Petrovic A.G., Abzalimov R., Paz M.M. and Champeil E. Synthesis of Oligonucleotides containing the cis-Interstrand Crosslink Produced by Mitomycins in their Reaction with DNA. *Chem. Eur. J., 2020;* (55):12570-12578. doi: 10.1002/chem.202002452. PMID: 32574396; PMCID: PMC7681910.
34. Zyss D., Montcourrier P., Vidal B., Anguille C., Mérezègue F., Sahuquet A., Mangeat P.H. and Coopman P.J. The Syk tyrosine kinase localizes to the centrosomes and negatively affects mitotic progression. *Cancer Res.* 2005 (65):10872-10880. doi: 10.1158/0008-5472.CAN-05-1270. PMID: 16322234.
35. Schindelin J., Arganda-Carreras I., Frise E., Kaynig V., Longair M., Pietzsch T., Preibisch S., Rueden C., Saalfeld S., Schmid B., Tinevez J.Y., White D.J., Hartenstein V., Eliceiri K., Tomancak P. and Cardona A. Fiji: an open-source platform for biological-image analysis. *Nat Methods*. 2012 (9):676-682. doi: 10.1038/nmeth.2019. PMID: 22743772; PMCID: PMC3855844.
36. Liu Y., Zhang Z., Gao X., Ma Q., Yu Z. and Huang S. Rab8A promotes breast cancer progression by increasing surface expression of Tropomyosin-related kinase B. *Cancer Lett.* 2022 (535):215629. doi: 10.1016/j.canlet.2022.215629. Epub 2022 Mar 10. Erratum in: Cancer Lett. 2022 May 5:215701. PMID: 35278612.
37. Banin S., Moyal L., Shieh S., Taya Y., Anderson C.W., Chessa L., Smorodinsky N.I., Prives C., Reiss Y., Shiloh Y. and Ziv Y. Enhanced phosphorylation of p53 by ATM in response to DNA damage. *Science.* 1998 (281):1674-1677. doi: 10.1126/science.281.5383.1674. PMID: 9733514.
38. Ioannou M.S. and McPherson P.S. Regulation of Cancer Cell Behavior by the Small GTPase Rab13. *J Biol Chem*. 2016 (291):9929-9937. doi: 10.1074/jbc.R116.715193. Epub 2016 Apr 4. PMID: 27044746; PMCID: PMC4858996.
39. Mayr B. and Montminy M. Transcriptional regulation by the phosphorylation-dependent factor CREB. *Nat Rev Mol Cell Biol* 2001 (2): 599–609. doi.org/10.1038/35085068.
40. Cargnello M. and Roux P.P. Activation and function of the MAPKs and their substrates, the MAPK-activated protein kinases. *Microbiol Mol Biol Rev.* 2011 (75):50-83. doi: 10.1128/MMBR.00031-10. Erratum in: Microbiol Mol Biol Rev. 2012 Jun;76(2):496. PMID: 21372320; PMCID: PMC3063353.
41. Bousoik E. and Montazeri Aliabadi H. "Do We Know Jack" About JAK? A Closer Look at JAK/STAT Signaling Pathway. *Front Oncol.* 2018 (8):287. doi: 10.3389/fonc.2018.00287. PMID: 30109213; PMCID: PMC6079274.
42. Dempke W.C.M., Uciechowski P., Fenchel K. and Chevassut T. Targeting SHP-1, 2 and SHIP Pathways: A Novel Strategy for Cancer Treatment? *Oncology* 2018 (95):257-269. doi: 10.1159/000490106. Epub 2018 Jun 20. PMID: 29925063.
43. Shin S.Y., Kim C.G., Lim Y. and Lee Y.H. The ETS family transcription factor ELK-1 regulates induction of the cell cycle-regulatory gene p21(Waf1/Cip1) and the BAX gene in sodium arsenite-exposed human keratinocyte HaCaT cells. *J. Biol. Chem.*, 2011; (30): 26860-26872. doi: 10.1074/jbc.M110.216721. PMID: 21642427; PMCID: PMC3143646.
44. Park J.S., Qiao L., Gilfor D., Yang M.Y., Hylemon P.B., Benz C., Darlington G., Firestone P.B. and P. Dent. A role for both Ets and C/EBP transcription factors and mRNA stabilization in the MAPK-dependent increase in p21 (Cip-1/WAF1/mda6) protein levels in primary hepatocytes.

Mol. Biol. Cell, 2000; (9): 2915-2932. doi: 10.1091/mbc.11.9.2915. PMID: 10982390; PMCID: PMC14965.

45. Bellidao T., O'Brien C.A., Roberson P.K. and Manolagas S. C. Transcriptional activation of the p21(WAF1,CIP1,SDI1) gene by interleukin-6 type cytokines. A prerequisite for their pro-differentiating and anti-apoptotic effects on human osteoblastic cells. *J. Biol. Chem.*, 1998; (33): 21137-21144. doi: 10.1074/jbc.273.33.21137. PMID: 9694869.

46. De Keizer P.L., Packer L.M., Szypowska A.A., Riedl-Polderman P.E., Van Den Broek N. J., De Bruin A., Dansen T.B., Marais R., Brenkman A.B. and Burgering B.M. Activation of forkhead box O transcription factors by oncogenic BRAF promotes p21cip1-dependent senescence. *Cancer Res.*, 2010; (21): 8526-8356. doi: 10.1158/0008-5472.CAN-10-1563. PMID: 20959475; PMCID: PMC2989643.

47. Karkhanis M. and Park J.-I. Sp1 regulates Raf/MEK/ERK-induced p21(CIP1) transcription in TP53-mutated cancer cells. *Cell. Signal.*, 2015; (3): 479-486. doi: 10.1016/j.cellsig.2015.01.005. PMID: 25595558; PMCID: PMC4333010.

48. Child E.S. and Mann D.J. The intricacies of p21 Phosphorylation: Protein/Protein Interactions, Subcellular Localization and Stability. *Cell Cycle*, 2006; (12): 1313-1319. doi: 10.4161/cc.5.12.1863. PMID: 16775416.

49. Wang Z., Bhattacharya N., Mixter P.F., Wei W., Sedivy J., Magnuson N.S. Phosphorylation of the cell cycle inhibitor p21Cip1/WAF1 by Pim-1 kinase. *Biochim Biophys Acta*. 2002; (1):45-55. doi: 10.1016/s0167-4889(02)00347-6. PMID: 12431783.

50. Suzuki A., Kawano H., Hayashida M., Hayasaki Y., Tsutomi Y., Akahane K. Procaspase 3/p21 complex formation to resist fas-mediated cell death is initiated as a result of the phosphorylation of p21 by protein kinase A. *Cell Death Differ.* 2000; (8):721-728. doi: 10.1038/sj.cdd.4400706. PMID: 10918446.

51. Chiaradonna F., Balestrieri C., Gaglio D., Vanoni M. RAS and PKA pathways in cancer: new insight from transcriptional analysis. *Front Biosci.* 2008; (13): 5257-5278. doi: 10.2741/3079. PMID: 18508585.

52. Hwang C.Y., Lee C., Kwon K.S. Extracellular signal-regulated kinase 2-dependent phosphorylation induces cytoplasmic localization and degradation of p21Cip1. *Mol Cell Biol.* 2009; (12):3379-3389. doi: 10.1128/MCB.01758-08. PMID: 19364816; PMCID: PMC2698740.

53. Tang D., Wu D., Hirao A., Lahti J.M., Liu L., Mazza B., Kidd V.J., Mak T.W and Ingram A.J. ERK activation mediates cell cycle arrest and apoptosis after DNA damage independently of p53. *J Biol Chem.* 2002 (277):12710-12717. doi: 10.1074/jbc.M111598200. Epub 2002 Jan 30. PMID: 11821415.

54. Neise D., Sohn D., Stefanski A., Goto H., Inagaki M., Wesselborg S., Budach W., Stühler K., Jänicke R.U. The p90 ribosomal S6 kinase (RSK) inhibitor BI-D1870 prevents gamma irradiation-induced apoptosis and mediates senescence via RSK- and p53-independent accumulation of p21WAF1/CIP1. *Cell Death Dis.* 2013; (10): e859. doi: 10.1038/cddis.2013.386. PMID: 24136223; PMCID: PMC3920941.

55. Zhang Y., Wang Z., Magnuson N.S. Pim-1 kinase-dependent phosphorylation of p21Cip1/WAF1 regulates its stability and cellular localization in H1299 cells. *Mol Cancer Res.* 2007 (5): 909-22. doi: 10.1158/1541-7786.MCR-06-0388. PMID: 17855660.

56. Esposito F., Russo L., Chirico G., Ammendola R., Russo T., Cimino F. Regulation of p21waf1/cip1 expression by intracellular redox conditions. *IUBMB Life*. 2001; (1-2):67-70. doi: 10.1080/15216540252774793. PMID: 11795596.

Highlights

- Mitomycin C (MC) and its major ICL downregulate MAPK/ERK pathway in MCF-7
- MC analog (DMC) and its major ICL downregulate MAPK/ERK pathway in K562
- The stereochemistry of ICLs contributes to the differential regulation of MAPK/ERK
- JAK/STAT pathway is downregulated by MC/DMC treatment in both MCF-7 and K562
- RAB8A and RAB13 are potential molecular targets of MC/DMC ICLs

Declaration of interests

☐ The authors declare that they have no known competing financial interests or personal relationships that could have appeared to influence the work reported in this paper.

☒ The authors declare the following financial interests/personal relationships which may be considered as potential competing interests:

Elise Champeil reports financial support was provided by National Institutes of Health. If there are other authors, they declare that they have no known competing financial interests or personal relationships that could have appeared to influence the work reported in this paper.